NASA TT F-11,378

A STUDY ON THE LARGE SCALE AIR EJECTOR

Shoichi Fujii, Mitsuo Gomi and Noboru Sugahara

Translation of the following:
Technical Report of the National Aerospace Laboratory, NAL TR-109, Tokyo,, July 1966, 32 pages

NATIONAL AERONAUTICS AND SPACE ADMINISTRATION
WASHINGTON, D. C. 20546 JUNE 1968

A STUDY ON THE LARGE SCALE AIR EJECTOR

Shoichi Fujii, Mitsuo Gomi and Noboru Sugahara

ABSTRACT. The air ejector (length 7m, ejector diameter 6mm) was investigated experimentally and theoretically. Mass ratio range varied from 0 to 1.4, compression ratios from 1.03 to 1.38. The device is used with a single-stage axial flow compressor.

1. Introduction /1 *

Air ejectors have been employed in many fields of engineering for the following reasons. It may be regarded as a vacuum pump having low efficiency but very simple mechanical construction. It has no mechanically rotating parts, which makes it possible for the air ejector to be used with minimum maintenance costs. It has recently been used as vacuum equipment for the high altitude simulation of a rocket engine (Ref. 14).

One purpose of this research is to build a compressor with high axial velocity of the air stream. This was done by placing a large-scale air ejector at the end of a jet engine booster. It is necessary that an air compressor of a multi-stage jet engine be capable of handling high pressure air at each stage. It is also necessary that a test be performed on a rotating propellor in a high speed air stream. This large-scale air ejector was developed as a part of the above experiments. The authors have obtained many interesting results for the large-scale ejector, both in the design and in the theoretical analysis. These results will be presented in detail. /2

A great deal of research has been performed on ejectors since 1930. The fluids employed are not only air, but also vapor and water. The type of ejector, as well as its mechanical construction, varies depending upon the fluid employed. The ejector discussed in this paper is a center-jet type, air ejector with a compression ratio ranging from 1.2 to 1.4. It is a large-scale ejector about 7000mm in length.

There havebeen a great many reports on the design specifications and data for a small-scale air ejector (Ref. 1 - 3, 10 - 12). However, they must be modified when a large-scale ejector is to be developed. Kastner and Spooner (Ref. 2) successfully developed an ejector experimentally which was about 800mm in length, by making various combinations of area ratios and diffuser lengths. Manganiello and Bogatsky (Ref. 3) analyzed the experimental data on a square ejector 1000mm long; this ejector was developed for a cooling system for an aircraft engine. Takashima and Hasegawa (Ref. 10) reported on the experimental results and theoretical analysis of a supersonic ejector built for chemical engineering purposes. Miyata (Ref. 9) presented an outline of his experiment for a large-scale ejector, but the detailed data are not given here.

*Note: Numbers in the margin indicate pagination in the original foreign text.

Two fluids are mixed inside an ejector at different speeds. This produces very sophisticated aerodynamical and turbulent phenomena. The above research was performed from the macroscopic viewpoint, without considering the processes inside the ejectors. Watabe (Ref. 11, 12) and others reported upon experimental work investigating the pressure change on the wall of an ejector, but no analytical work was performed. On the other hand, a purely theoretical analysis of the phenomena inside an ejector has been made. The most typical analysis was that performed by Pai (Ref. 4). The authors studied a large-scale ejector and obtained experimental data about pressure changes and pressure distribution along the wall of a mixing tube. At the same time, theoretical analysis of the pressure changes was performed using the conservation of momentum of the fluid inside the mixing tube.

2. Aerodynamical Design Specifications of the Ejector

2.1 Performance

It is necessary that the secondary air flow is 20 kg/sec when the primary air flow is 20 kg/sec; i.e., the air flow ratio is set to be 1.0. Inside diameter of the mixing tube is set to be 600mm. Thus, the primary air will be choked and there will be a sonic air stream at the end of the nozzle. /3

2.2 Design Specifications

The following design specifications are set, mainly based upon the data for a small ejector reported by Kastner and Spooner (Ref. 2). All symbols used are the same as those shown in Figure 1.

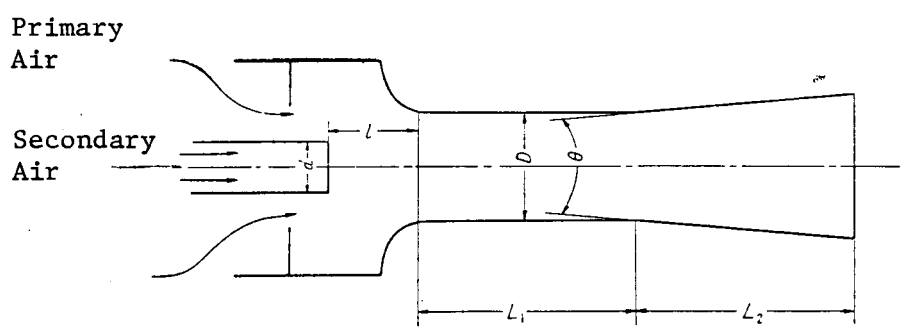

Figure 1. Symbols for Each Part.

2.2.1 Ratio of Mixing Tube Area to Driving Nozzle Area $(D/d)^2$

This value is a very important factor for the overall capability of an ejector. Experiments were performed for two different values: one is $(D/d)^2 = 9.0$, and the other is 6.8. Thus, for the mixing tube of D = 600mm, two nozzles were prepared, d = 200, and 230mm.

2.2.2 Ratio of Length of Mixing Tube to Inside Diameter of Mixing Tube L_1/D

If L_1 is too small, two streams of air pass into the diffuser which are

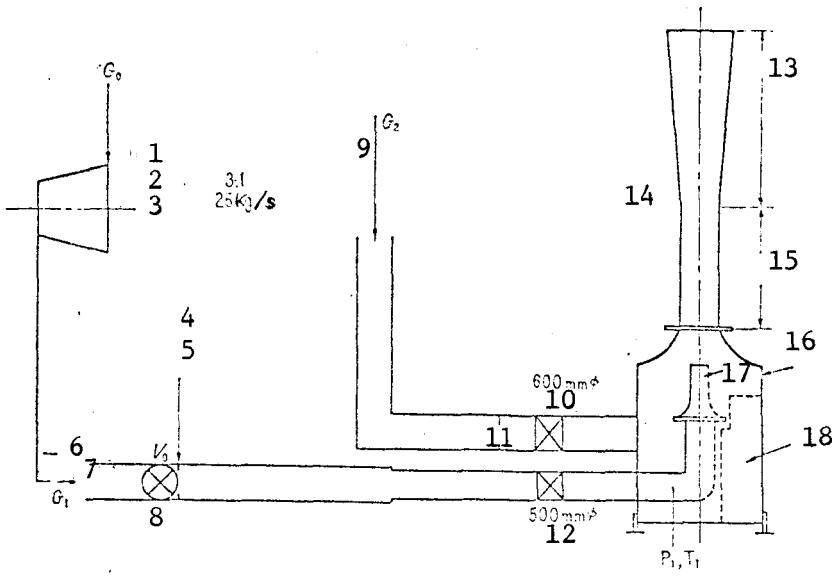

Figure 2. Experimental Apparatus

1. 10 Stage Compressor
2. Pressure Ratio
3. Stream Rate
4. Primary Air
5. Flow Meter
6. Primary Air
7. (Moving Air)
8. Funnel Valve
9. Secondary Air
10. Control Valve
11. Orifice
12. Control Valve
13. Diffuser
14. Main Body of Ejector
15. Parallel Section of Mixing Tube
16. Chamber
17. Nozzle
18. Baffle Blade

insufficiently mixed with each other. On the other hand, if L_1 is too large, the overall capability of the ejector will be lowered. It is reported that L_1/D = = 7.0~8.0 could be the optimal value for a small ejector. If this value is used for a large-scale ejector, then the length of the ejector becomes very great. Thus, the value L_1/D is chosen to be 4.0. This could be a reasonable value which would not harm the overall capability of the ejector.

2.2.3 Distance Between Nozzle and Mixing Tube

Let 1/D be defined as the projection ratio. For the value of L_1/D=4.0, the projection ratio 1/D = 1.0 could be the most reasonable value. Therefore, a long nozzle was prepared for the experiment, and it was shortened during the experiment. Data were obtained for the value of 200mm through 660mm. Therefore, the value of 1/D ranged from 0.33 to 1.10.

2.2.4 Angle of Diffuser θ

When the value of the real ratio $(D/d)^2$ is less than 25, this angle θ is very important and should not exceed the value of 10°. It is recommended that it lie somewhere between 5° and 10°. In this experiment θ is set to be 6°.

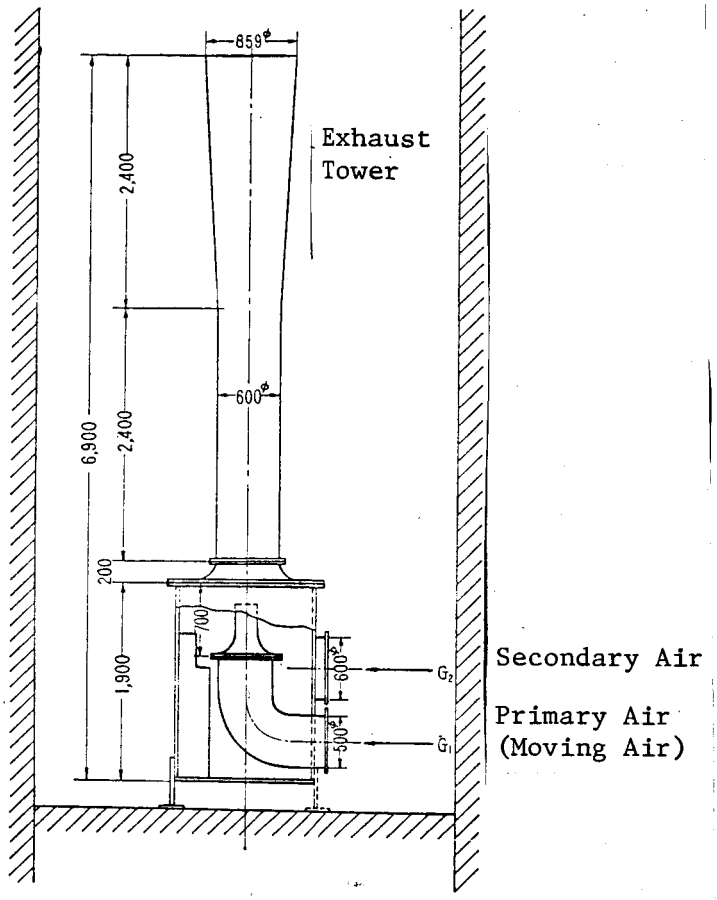

/4

Figure 3. Main Body of Ejector

TABLE I. SHAPE OF EJECTOR ACCOMPANYING EXPERIMENT

Experiment No. (Main Classification)	Nozzle d Diameter	Area Ratio $(D/d)^2$	Distance Between Tip of Nozzle and Parallel Section l
10x	200mm	9.00	200mm
60x	200	9.00	400
20x	200	9.00	600
30x	230	6.81	200
40x	230	6.81	430
50x	230	6.81	660

3. Experimental Apparatus

/5

The entire apparatus is shown in Figure 2. For the driving air (primary air), air was compressed by the 10-stage axial flow compressor which has a compression ratio of 3.1, and a capacity of 25 kg/sec air flux. The driving air passes through a rotary valve, and an inlet regulating valve for flux measurement

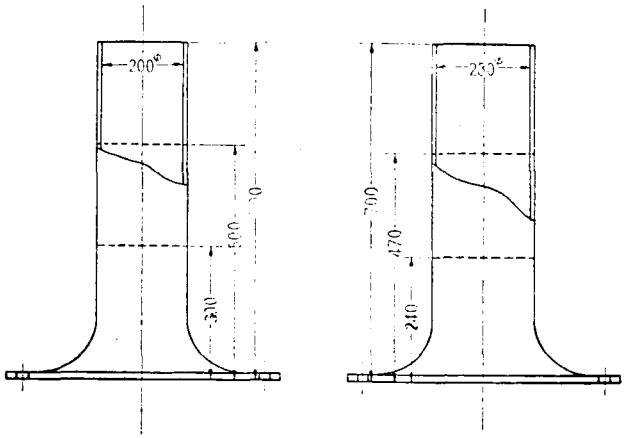

Figure 4. Nozzle

and control, and is then ejected from the nozzle in the chamber. On the other hand, the intake air (secondary air) is sucked in from the atmosphere, passes through a 600mm diameter air tube, and flows into the chamber after its flow rate is adjusted by the regulating valve. A baffle plate is installed in order to prevent rotational motion of the secondary air. When using a single-stage compressor, the compressor outlet is connected to the end of the 600mm diameter tube on the secondary side. As shown in Figure 3, the ejector consists of a chamber, a nozzle, a mixing tube, and a diffuser. It is installed in the vertical position inside the evacuation tower for the air turbine.

4. Experimental Methods and Measurements

The dimensions of the ejectors used in the experiments are shown in Table I. Experiments were carried out keeping the sizes of the mixing tube and the diffuser constant, but varying the nozzle diameter (hence, the area ratio $(D/d)^2$ of the mixing tube and the nozzle) and also l the distance from the tip of the nozzle to the parallel part of the mixing tube. In Table I, entries 10x, 20x indicate that the experiment numbers of the data on the various ejectors are in the 100 and 200 series. As shown in Figure 4, fine tip nozzles were used; they were cut at the tip at the dotted line in order to vary l. As mentioned before, the flow rate of the driving air was measured by the flowmeter which was mounted on the rotary valve. Then, after the flow rate was further adjusted by the regulating valve to the desired flow rate, the total temperature and pressure were measured by the total temperature and pressure tube just prior to ejection from the nozzle. The flow rate of the intake air was measured by an orifice mounted in front of the regulating valve. As shown in Figure 5, a total of 23 static pressure holes of 1mm diameter were mounted in the walls: 5 in the diffuser; 15 in the mixing tube (3 places around the periphery at both the inlet and outlet of the parallel part); 1 in the bellmouth at the mixing tube inlet; 2 in the chamber. In order to measure the total pressure, 2 total pressure Pitot tubes /8 were inserted in the chamber, and comb-shape Pitot tubes were inserted in the inlet and outlet of the mixing tube straight part. Photographs 2 and 3 show the external view of the mixing tube together with part of the diffuser, and the bellmouth portion of the mixing tube inlet together with the chamber, respectively. The static pressure was led to the outlet of the evacuation tower by copper tubes, from where it was led to the mercury manometer by vinyl tubes. Pressures connected to flow rates -- such as the orifice differential pressure and its static pressure -- were measured by a pressure gauge which has a Bordon tube. The temperatures were measured with iron-constantan thermocouples. In Photograph 4, the lower right shows the primary air tube before the chamber, and the lower left shows the secondary air tube and its regulating valve.

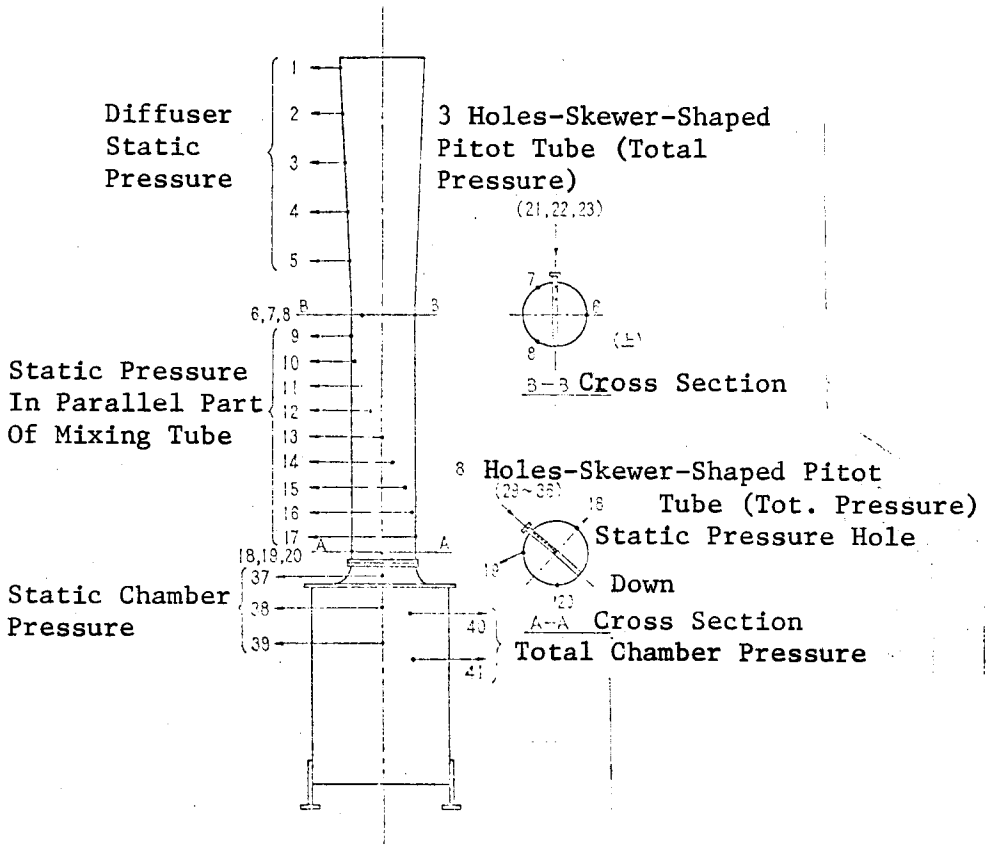

Figure 5. Position of Static Pressure Measuring Holes and Total Chamber Pressure

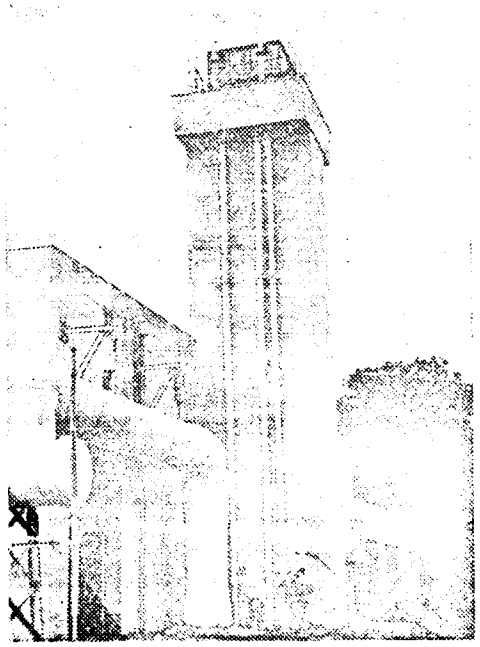

Photo. 1. Evacuation Tower Which Houses the Ejector.

Photo. 2. Mixer Tube and Diffusor

/7

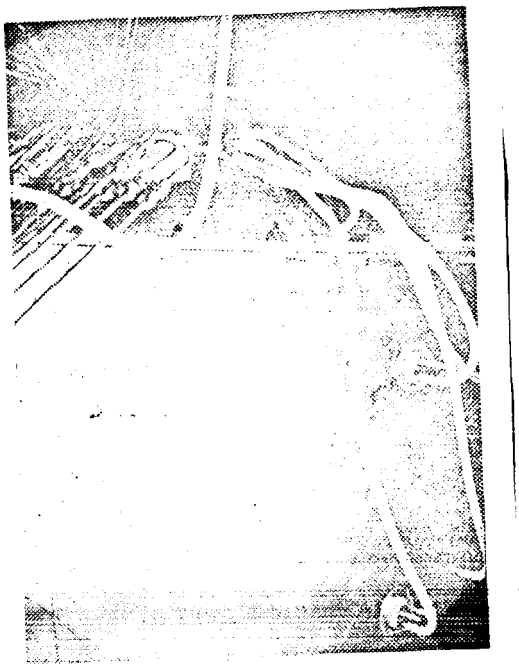

Photo. 3. Chamber and Bellmouth.

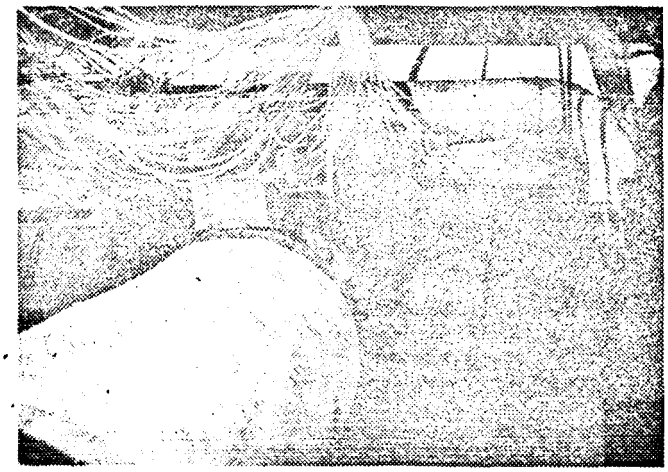

Photo. 4. Primary and Secondary Air Tube.

5. Experimental Results on the Total Performance /8

The most common way to express the total performance of the ejector is to compare the degree of vacuum or the compression ratio with the flux ratio. Compression ratio is the ratio of the atmospheric pressure to the static pressure in the chamber, whereas the flux ratio is the value obtained by dividing the intake air flux by the driving air flux. The compression ratios are plotted against flux ratios in Figures 6 and 7. Three driving fluxes were used as parameters instead of the driving pressures, which are often given in other reports, in order that the primary flow rate can be directly read on a flowmeter. When the nozzle diameters are 200mm (Figure 6) and 230mm (Figure 7), the fluxes are G_1 = 17.0 kg/sec, and 21.2 kg/sec, respectively, (maximum driving air fluxes). They either correspond to choked conditions or 0.2 kg/sec less than choked conditions. That is, since the inlet condition (atmospheric pressure, temperature) of the compressor, which furnishes the driving air, varies from day to day, the maximum air flux varies even though the nozzle diameter is constant. When measurements are made near the maximum driving flux, a slightly lower flux than the maximum obtainable one is used when the atmospheric temperature is slightly lower than usual. The flux ratio m = 0 holds when the intake inlet valve is completely closed, whereas the maximum value of m is determined by the resistance of the intake tube when the inlet valve is completely open. The higher the driving flux, the higher the pressure ratio is, and hence the vacuum. The highest vacuum obtained in this experiment was -207 mm Hg (gauge pressure). As the flux ratio increases, the compression ratio necessarily decreases, which is large when the driving flux is large. Although the compression ratio is low when the driving flux is small, the flux ratio, on the contrary, increases. When G_1 = 6.4 kg/sec, the maximum value of m is 1.42 (Figure 6). The relation between the driving flux

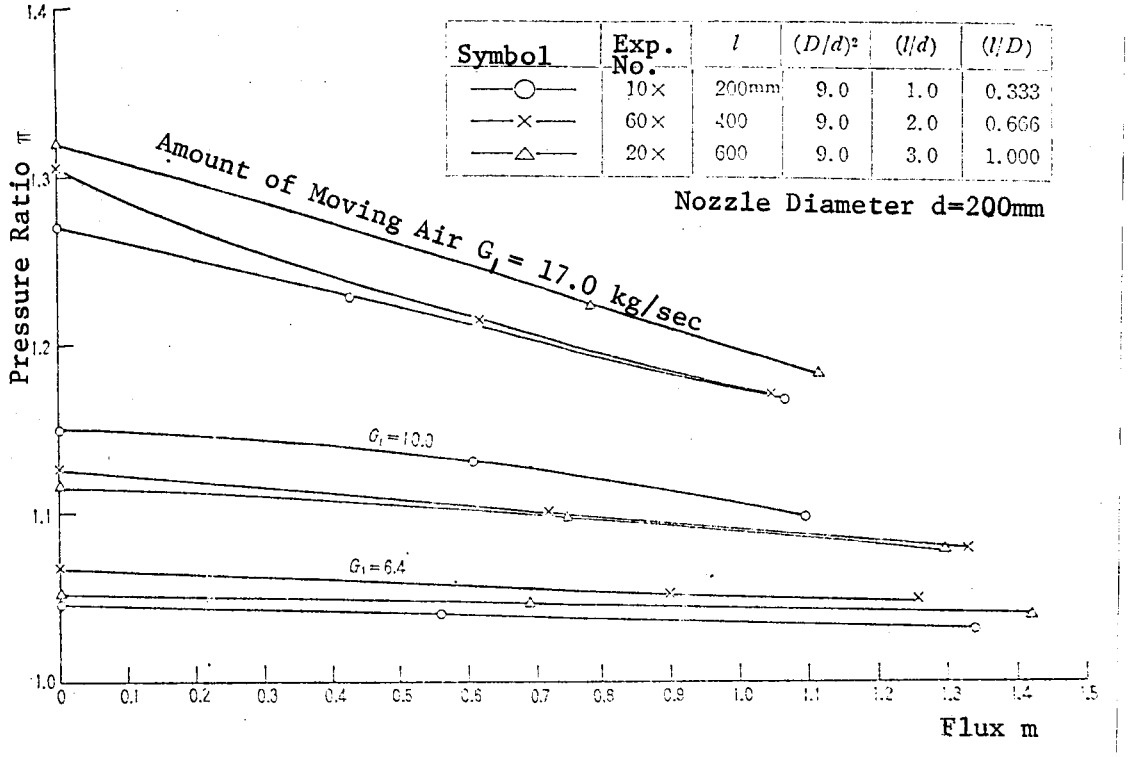

Figure 6. Flux Ratio and Pressure Ratio (a1).

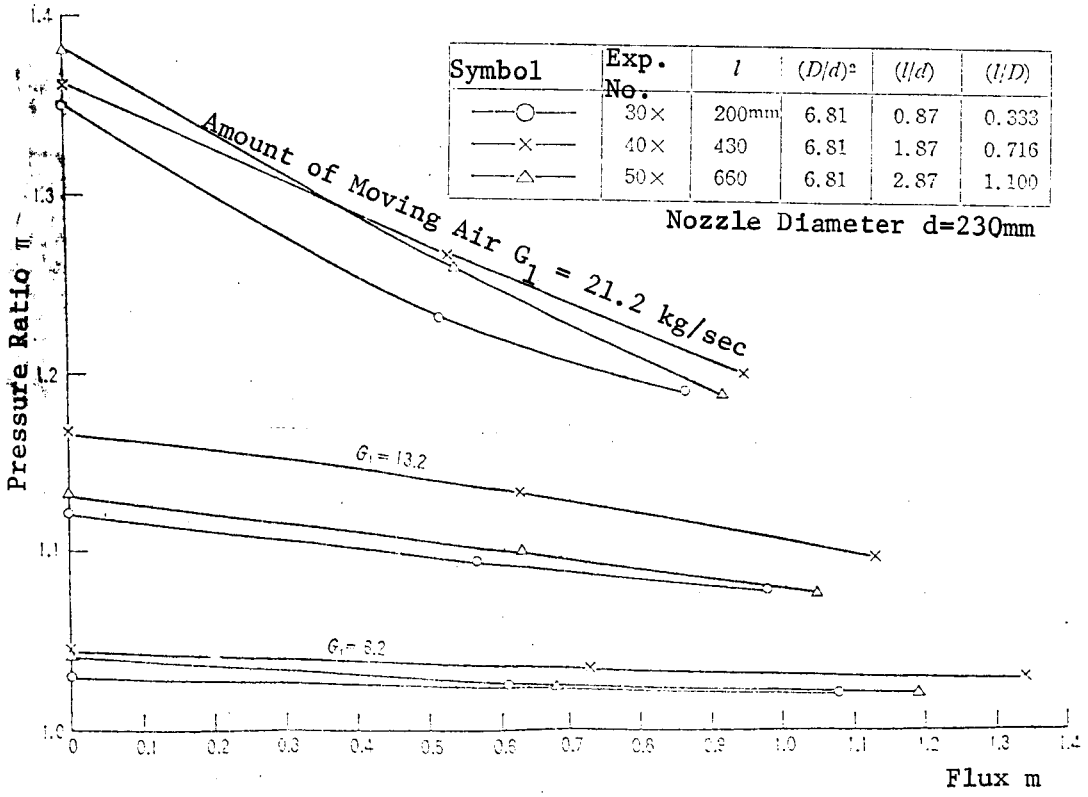

Figure 7. Flux Ratio and Pressure Ratio (b2).

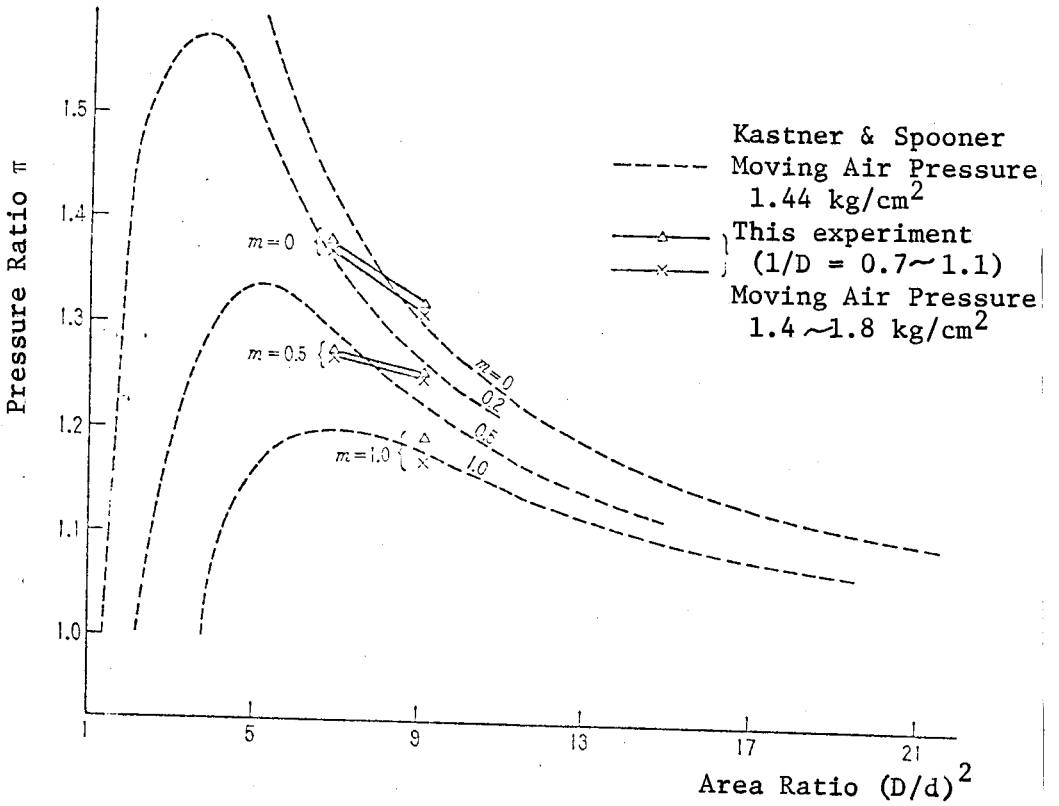

Figure 8. Area Ratio and Pressure Ratio.

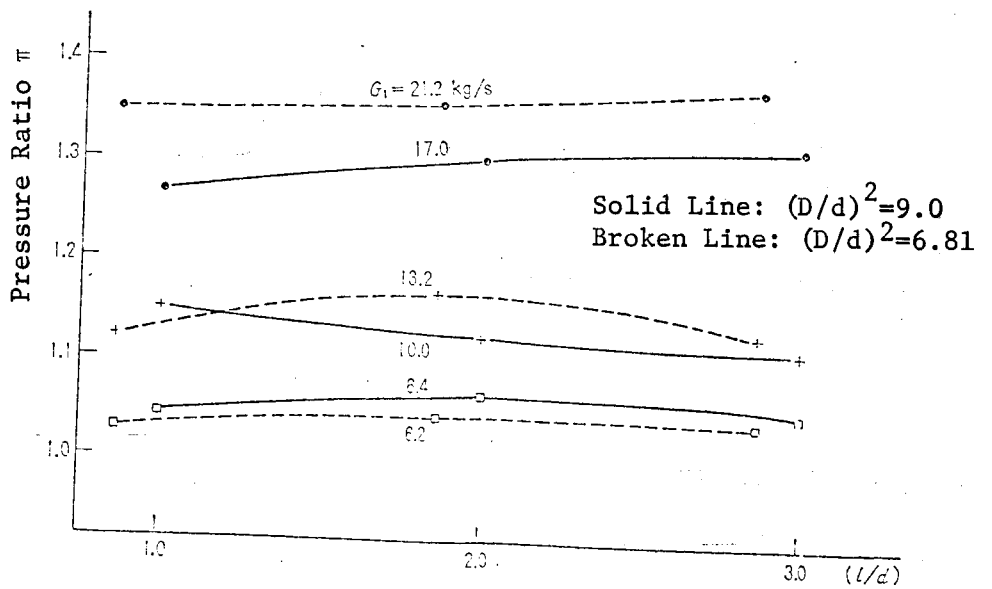

Figure 9. (Length From Nozzle to Mixing Tube) and (Nozzle Diameter).Pressure Ratio.

and the total pressure just prior to nozzle ejection is shown in Table II, in which the approximate pressures are indicated since they vary from day to day. Figure 8 shows the relationship between the area ratio and the compression ratio using the flux ratio as a parameter. Our data are compared with the curves obtained by Kastner and Spooner.

TABLE II. RELATIONS BETWEEN AMOUNT OF MOVING AIR AND MOVING PRESSURE AT THE SAME TIME

Amount of Moving Air G_1	Moving Air Pressure (gauge)	Amount of Moving Air G_1	Moving Air Pressure (gauge)
17.0 kg/sec	1.6~1.8 kg/cm^2	21.2 kg/sec	1.4~1.6 kg/cm^2
10.0	0.6~0.8	13.2	0.5~0.7
6.4	0.16~0.21	6.2	0.15~0.17

Since we were unable to obtain experimental data corresponding to the area ratio $(D/d)^2 = 6.81$, and driving pressure of approximately 1.4 kg/cm^2 when $m = 1.0$, only data for $(D/d)^2 = 9.0$ are shown. They approximately agree with the values obtained for small ejectors. When $m = 0$, 0.5, even though the absolute values of the slopes are smaller in our experiment, the values themselves do not appreciably differ from the curves. The relations between 1/d and the compression ratio, using the driving flux as a parameter, are shown in Figure 9. With either nozzle, when the driving flux is maximum, the compression ratio is higher, the higher is 1/d -- that is, the shorter the nozzle length, the higher is the vacuum. In the experiment when the driving flux was at the maximum, very loud noises accompanied by rumbling vibrations were generated as a result of the expansion of the jets at the nozzle which reach supersonic speed locally. When the driving flux was low, primarily low frequency sounds were audible with hardly any vibration. Since the jets from the nozzle are either sonic or subsonic flows at such a low driving flux, as is evident from Table II, (1/d) = 2.0 is sufficiently long to effect a high vacuum. /11

Ejectors are classified into two categories, according to their usage depending on whether they require a high vacuum or whether they are used to obtain high flow rates. Since in this experiment they are used for the latter purpose, we need to examine the relationships between the projection ratio and the flux ratio as shown in Figure 10. The compression ratio is used as a parameter in this figure, which shows that when the projection ratio is the same, the smaller the compression ratio, the higher is the flux ratio. /12

When $(D/d)^2 = 9.0$, better results were obtained at high projection ratios. A flux ratio, $m = 0.95$ (Point A in Figure 10) was obtained when the compression ratio was $\pi = 1.20$, and the projection ratio was $1/d = 1.0$. Although $m = 1.0$ was expected from the design, a value which is 0.05 less was obtained. When $(D/d)^2 = 6.81$, the maximum flux ratio was obtained in the vicinity of $1/D = 0.7$. A further increase in the projection ratio is undesirable from the flow rate standpoint.

In Figures 11, 12, and 13, the degree of vacuum as a function of the primary

/11

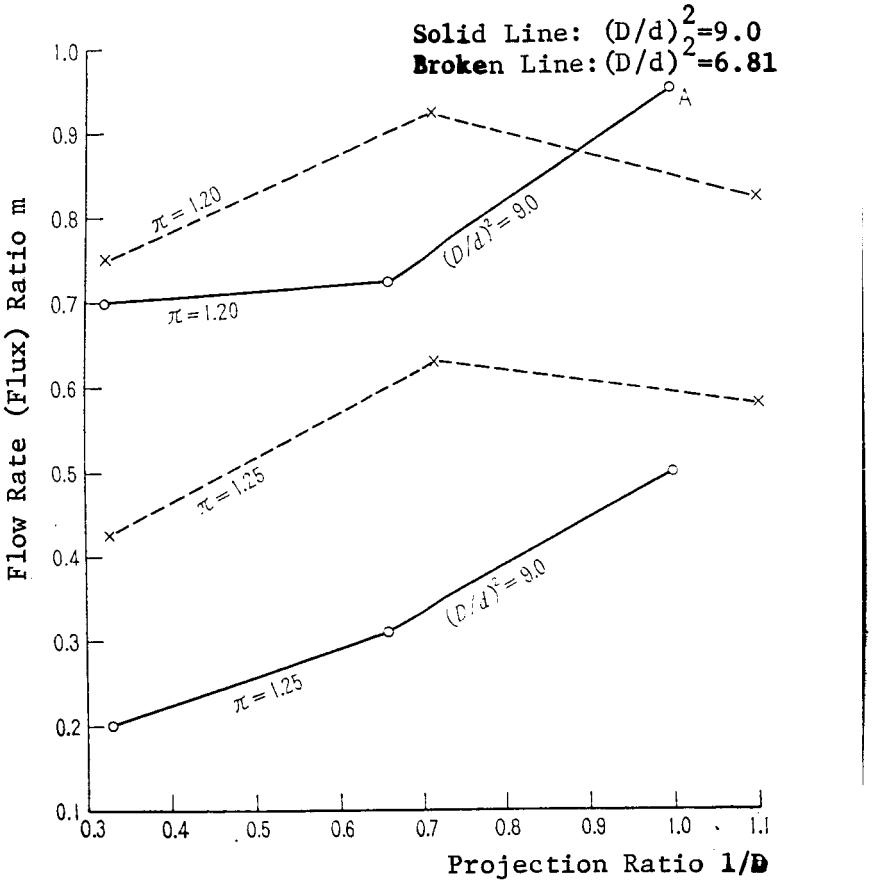

Figure 10. Projection Ratio and Flow Rate (Flux) Ratio.

/12

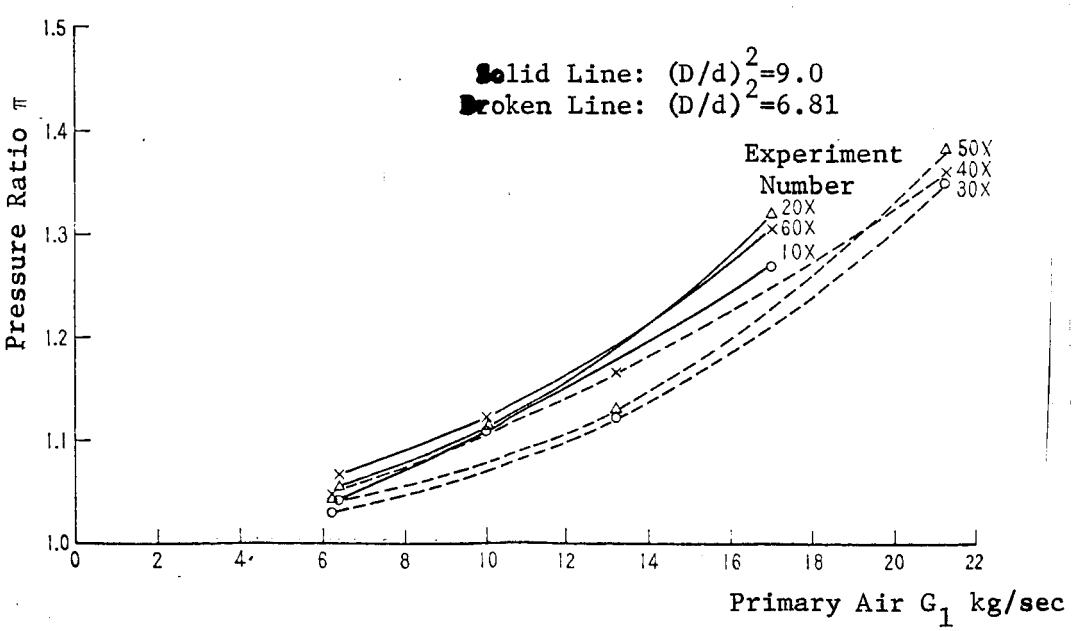

Figure 11. Amount of Primary Air and Pressure Ratio (m = 0)

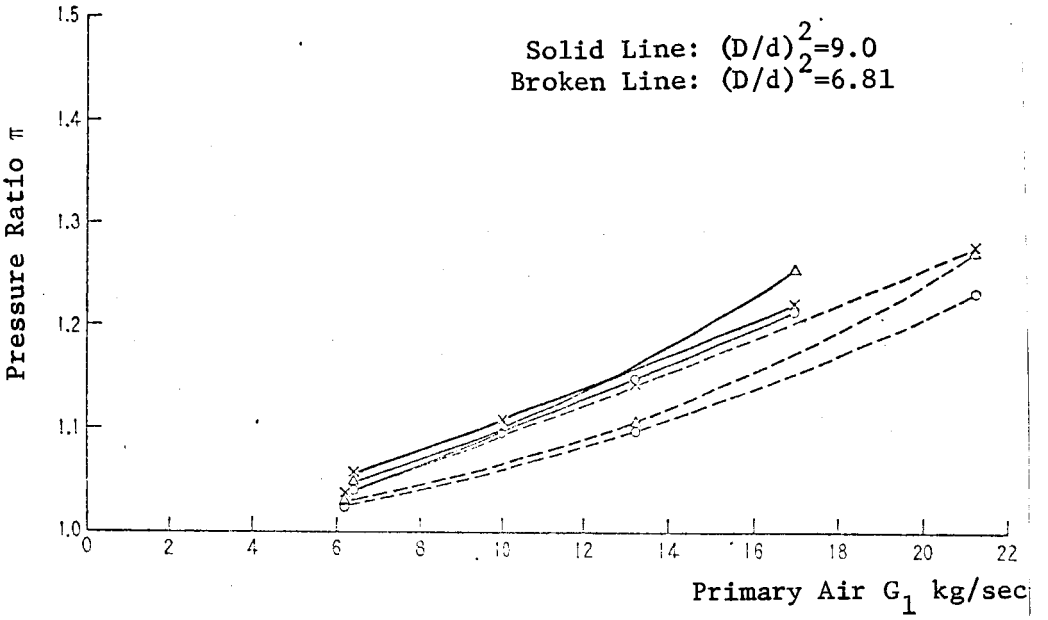

Figure 12. Amount of Primary Air and Pressure Ratio (m = 0.5)

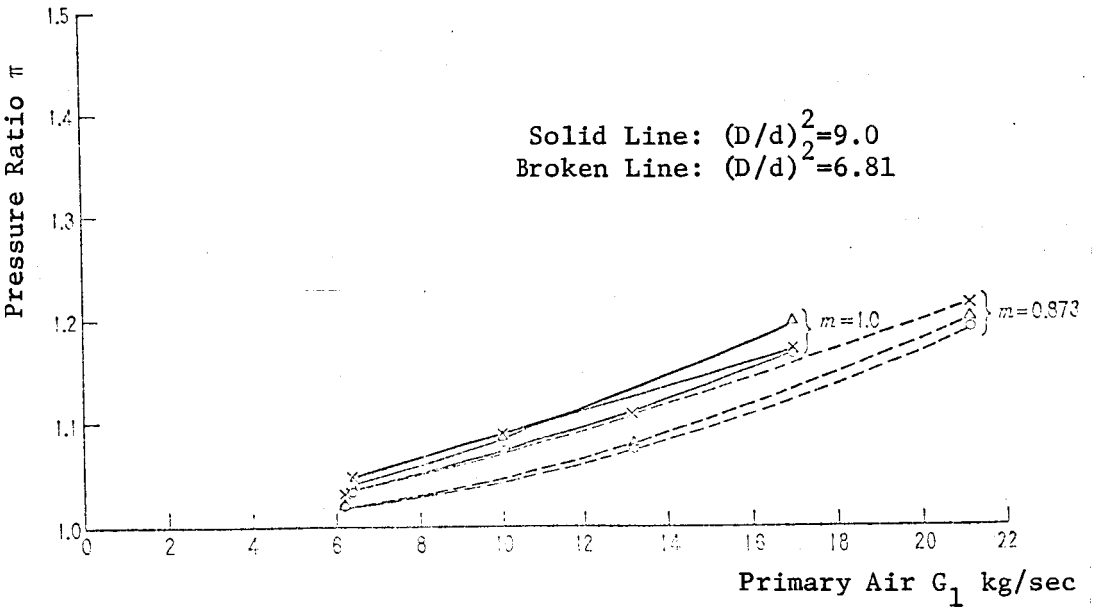

Figure 13. Amount of Primary Air and Pressure.

air flux is shown. Figure 11 shows how the vacuum increases with the driving flux when the flux ratio m = 0. Figure 12 shows the changes when m = 0.5. In Figure 13, when the area ratio $(D/d)^2$ = 9.0, m = 1.0 is used to show the changes. When $(D/d)^2$ = 6.81, m = 0.873 was used, since we were unable to obtain m = 1.0. In all cases, with the same driving flux, the larger the area ratio, the larger is the compression ratio. Further, the smaller the flux ratio, the larger is the slope.

Figures 14 - 19 present the wall pressure distributions along the entire

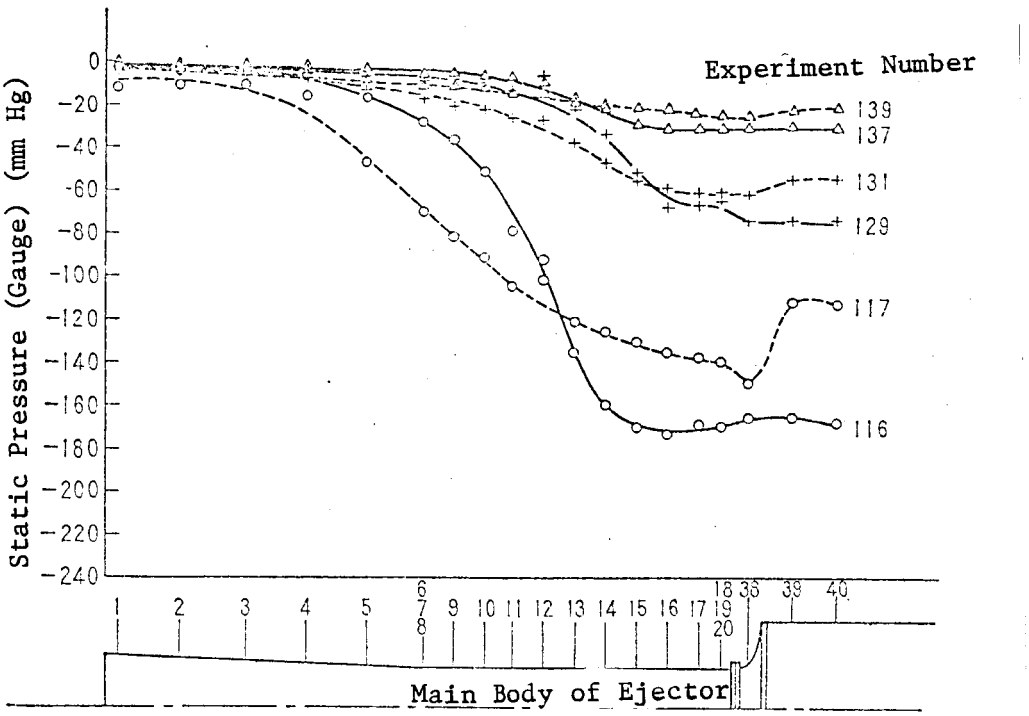

Figure 14. Static Pressure Distribution (a1).

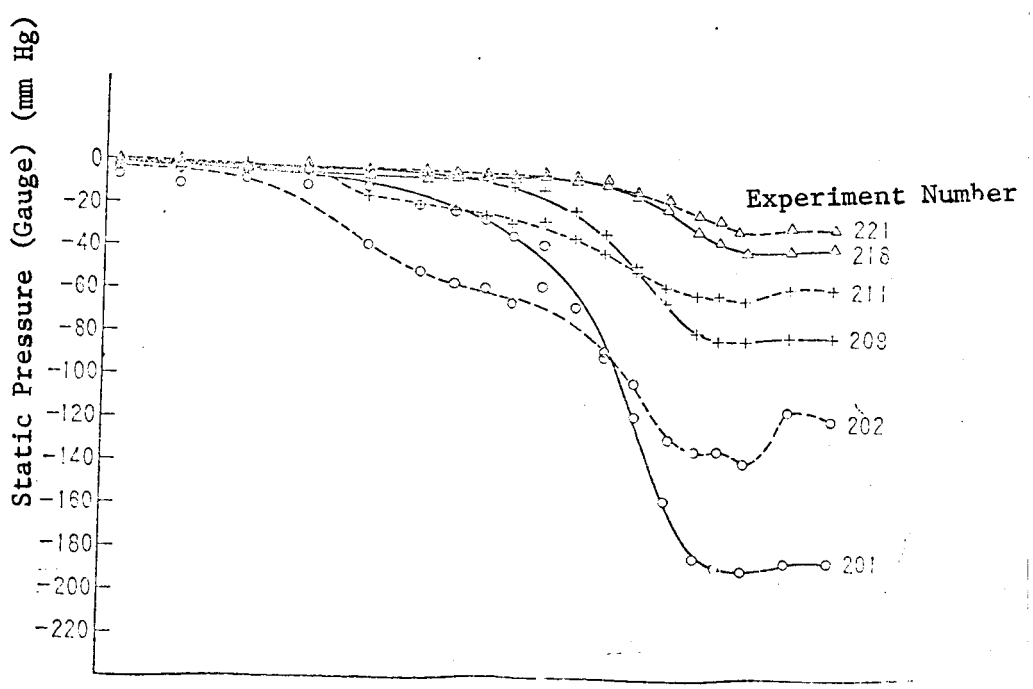

Figure 15. Static Pressure Distribution (b2).

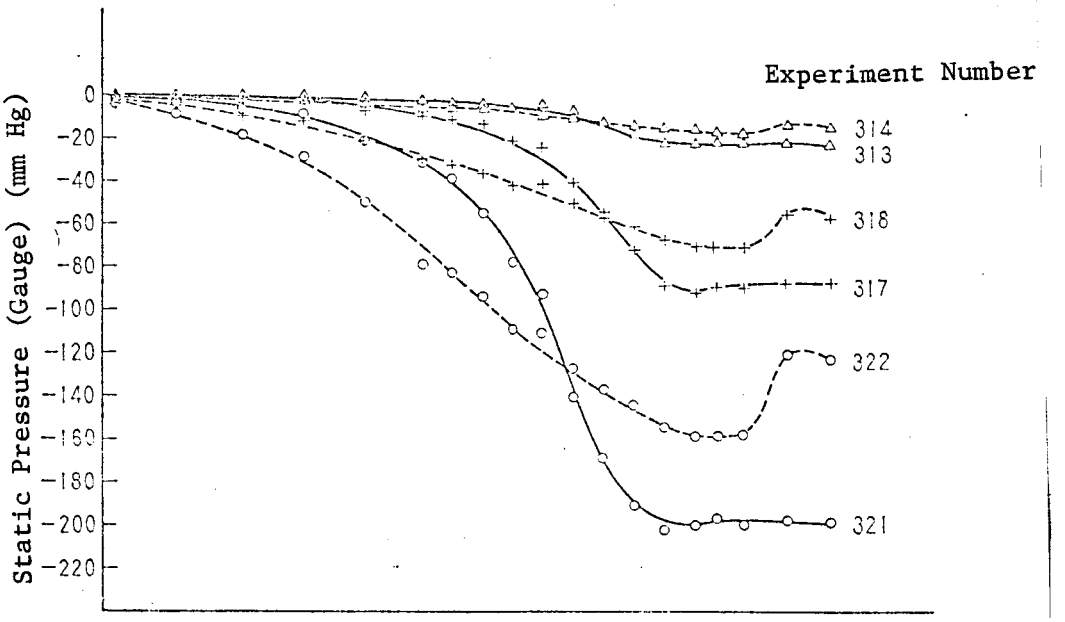

Figure 16. Static Pressure Distribution (c3).

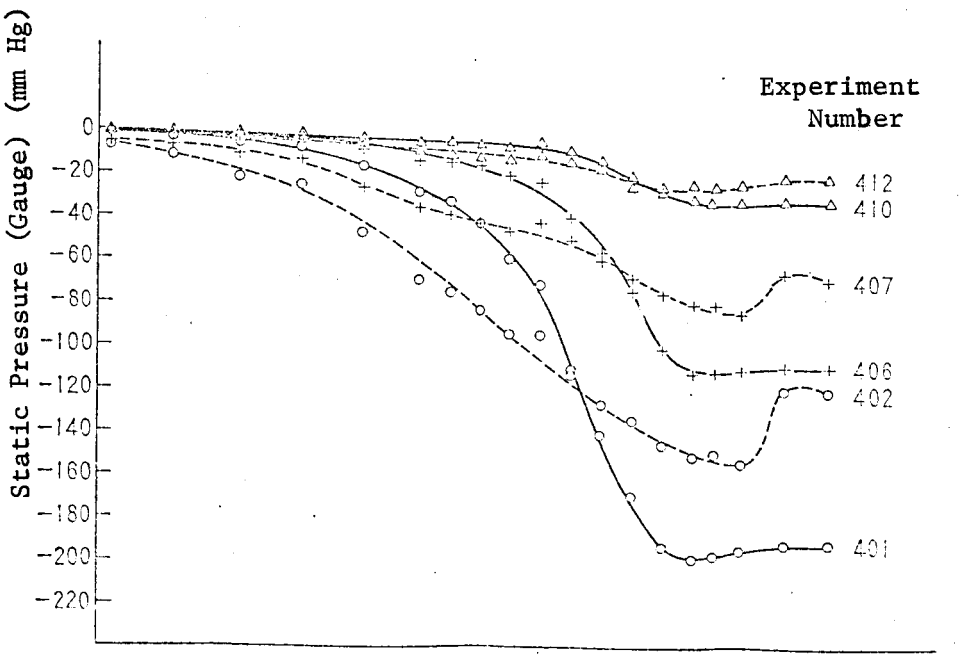

Figure 17. Static Pressure Distribution (d4).

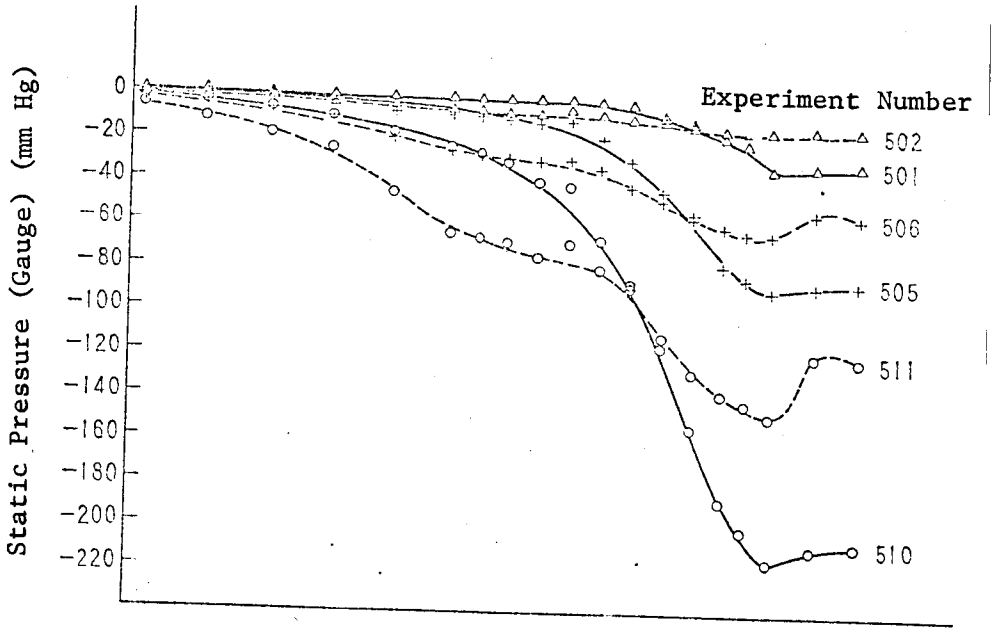

Figure 18. Static Pressure Distribution (e5).

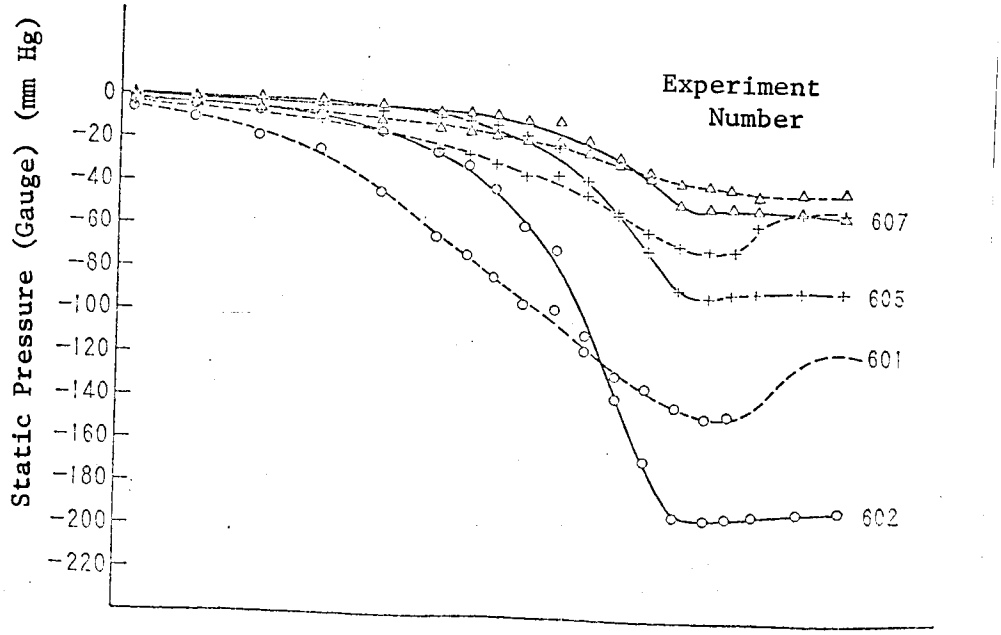

Figure 19. Static Pressure Distribution (f6).

ejector. Distances are plotted along the abscissa, and the gauge pressures in mm Hg are plotted along the ordinate. In Figure 14, the static pressures for m = 1.0 are plotted for Experiment Numbers 116, 129, 137. In Experiment Number 117, a pressure decrease is seen at the bellmouth due to the large secondary flow which is accelerated at the bellmouth. The pressure distributions from the chamber to the ejector outlet show the effectiveness of the diffuser. Similar conclusions can be derived from other figures.

6. Mixing Process

/17

6.1 Theory of Ducted Flow***

When the area of the mixing tube is constant in the longitudinal direction, the mixing is accompanied by a static pressure rise. The simplest way to calculate this static pressure rise is to invoke the principle of the conservation of momentum at the entrance and the exit, disregarding any intermediate process (Ref. 2,3). In this report, however, we will examine the mixing process a little more in detail by postulating a velocity profile.

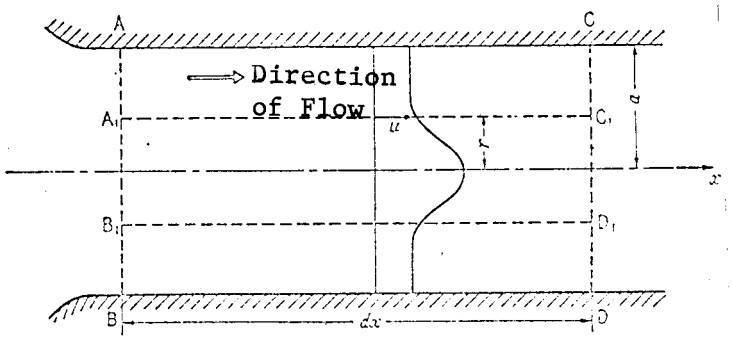

Figure 20. Mixing Tube.

Applying the principle of the conservation of momentum at plane $[A_1B_1D_1C_1]$ in Figure 20, and assuming that the static pressure p can be expressed only as a function of the axial coordinate x, we find

$$2\pi\frac{\partial}{\partial x}\left[\int_0^r \rho u^2 r\,dr\right]dx - u2\pi\frac{\partial}{\partial x}\left[\int_0^r \rho u r\,dr\right]dx = -\frac{dp}{dx}\pi r^2 dx - 2\pi r\,dx\cdot\tau \quad (1)$$

where u is the axial velocity at the point with the radial coordinate r. ρ is the density; τ is the apparent shearing stress of the turbulent flow. Letting a be the radius of the mixing tube, and substituting a dimensionless quantity $\eta = r/a$, equation 1 becomes,

$$\frac{\partial}{\partial x}\int_0^r \rho u^2\eta\,d\eta - u\frac{\partial}{\partial x}\int_0^r \rho u\eta\,d\eta = -\frac{dp}{dx}\cdot\frac{\eta^2}{2} - \frac{\tau\eta}{a} \quad (2)$$

Hence, an axial velocity profile must be postulated. Squire and Torouncer (Ref. 6) postulated a cosine curve velocity profile, not for ducted flows, but for jets in an infinitely wide free flow. Hill (Ref. 7) studied turbulent flows in a duct, and obtained an axial velocity profile by using values derived from experimental values obtained on jets in a free flow. At any rate, the differences

***Refer to Appendix 1 for the case of free flow.

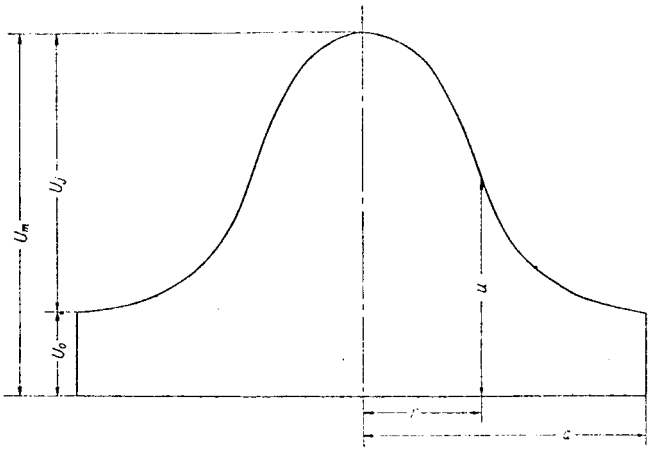

Figure 21. Velocity Distribution.

in the velocity profiles can be attributed to the mixing length. In reference to Figure 21, let us set

$$u = U_j[\lambda + f(\eta)] \tag{3}$$

$$\lambda = \frac{U_0}{U_j} \tag{4}$$

Assume η which is a function of f(η) to be a third order polynomial, and letting f(1) = f'(1) = f'(0) = 0, and f(0) = 1, we have

$$f(\eta) = 1 - 3\eta^2 + 2\eta^3 \tag{5}$$

Let us assume that the density varies linearly in the axial direction, but is constant in the radial direction. This can be expressed as

$$\frac{\rho}{\rho_0} = \left(\frac{x}{x_0}\right)\left(1 - \frac{\rho_i}{\rho_0}\right) + \left(\frac{\rho_i}{\rho_0}\right) \tag{6}$$

where ρ_o is the density at the ejector outlet, ρ_i is the density just prior to mixing which accompanies the pressure rise, x_o is the distance from where the mixing started to the ejector outlet, and ρ is the density at a distance x.

The following equation is obtained by substituting equation (3) into equation (2),

$$\begin{aligned} &\lambda'\left[\eta^2\lambda + 2\alpha_{1\eta} - (\lambda+f)\frac{\eta^2}{2}\right] \\ &+ \frac{U_j'}{U_j}\left[\eta^2\lambda^2 + 4\alpha_{1\eta}\lambda + 2\alpha_{2\eta} - (\lambda+f)\lambda\frac{\eta^2}{2} - (\lambda+f)\alpha_{1\eta}\right] + p'\left[\frac{\eta^2}{2\rho U_j^2}\right] \\ &= -\frac{\eta}{\rho U_j^2}\frac{\tau}{a} - \frac{\eta^2}{2}\frac{\rho'}{\rho}\lambda^2 - 2\alpha_{1\eta}\frac{\rho'}{\rho}\lambda - \alpha_{2\eta}\frac{\rho'}{\rho} + (\lambda+f)\lambda\frac{\eta^2}{2}\frac{\rho'}{\rho} + (\lambda+f)\alpha_{1\eta}\frac{\rho'}{\rho} \end{aligned} \tag{7}$$

where /19

$$\alpha_{1\eta} = \int_0^\eta \eta f(\eta)\, d\eta \tag{8}$$

$$\alpha_{2\eta} = \int_0^\eta \eta f^2(\eta)\, d\eta \tag{9}$$

The prime (') indicates differentiation.

As is evident from equation (7), three equations are necessary since there are three unknowns, λ', U_j'/U_j, and p'. Since equation (2), or equation (7) is a general equation derived at cross section $A_1B_1D_1C_1$ in Figure 20, by applying it to the cross section η = 1/2, we obtain

$$\lambda'\left(\frac{1}{8}\lambda+2\alpha_{12}-\frac{1}{16}\right)$$
$$+\frac{U_j'}{U_j}\left(\frac{1}{8}\lambda^2+3\alpha_{12}\lambda+2\alpha_{22}-\frac{1}{16}\lambda-\frac{1}{2}\alpha_{12}\right)+p'\left(\frac{1}{8\rho U_j^2}\right) \tag{10}$$
$$=-\frac{1}{2\rho U_j^2}\frac{\tau}{a}-\alpha_{12}\frac{\rho'}{\rho}\lambda-\alpha_{22}\frac{\rho'}{\rho}+\frac{1}{16}\frac{\rho'}{\rho}\lambda+\frac{1}{2}\frac{\rho'}{\rho}\alpha_{12}$$

where

$$\alpha_{12}=\int_0^{\frac{1}{2}}\eta f(\eta)d\eta=0.091 \tag{11}$$

$$\alpha_{22}=\int_0^{\frac{1}{2}}\eta f^2(\eta)d\eta=0.085 \tag{12}$$

Using the mixing length l, τ can be written as,

$$\tau=-\frac{\rho l^2}{a^2}\left(\frac{\partial u}{\partial \eta}\right)^2_{\eta=\frac{1}{2}} \tag{13}$$

Further, assuming that the mixing distance l can be written as follows, using an experimentally determined constant c, we have

$$l=c\alpha \tag{14}$$

Neglecting friction at the mixing tube wall, the following equation holds for the cross section $\eta = 1$

$$\lambda'(\lambda+2\alpha_1)+\frac{U_j'}{U_j}(\lambda^2+4\alpha_1\lambda+2\alpha_2)+p'\left(\frac{1}{2\rho U_j^2}\right)$$
$$=-\frac{1}{2}\frac{\rho'}{\rho}\lambda^2-2\alpha_1\frac{\rho'}{\rho}\lambda-\alpha_2\frac{\rho'}{\rho} \tag{15}$$

where

$$\alpha_1=\int_0^1\eta f(\eta)d\eta=0.150 \tag{16}$$

$$\alpha_2=\int_0^1\eta f^2(\eta)d\eta=0.086 \tag{17}$$

On the other hand, the flow rate m_1 of the mixing tube can be expressed as

$$\frac{m_1}{\pi a^2}=2\rho U_j(0.5\lambda+\alpha_1) \tag{18}$$ /20

from which we obtain

$$0.5\lambda'+\frac{U_j'}{U_j}(0.5\lambda+\alpha_1)=-\frac{\rho'}{\rho}(0.5\lambda+\alpha_1) \tag{19}$$

From equations (10), (15), and (19), we can write

$$\begin{pmatrix} \beta_1 & \beta_2 & \beta_3 \\ \beta_4 & \beta_5 & \beta_6 \\ \beta_7 & \beta_8 & \beta_9 \end{pmatrix} \begin{pmatrix} \lambda' \\ \dfrac{U_j'}{U_j} \\ p' \end{pmatrix} = \begin{pmatrix} \gamma_1 \\ \gamma_2 \\ \gamma_3 \end{pmatrix} \tag{20}$$

where

$$\left.\begin{aligned}
&\beta_1=\lambda+2\alpha_1 \\
&\beta_2=\lambda^2+4\alpha_1\lambda+2\alpha_2 \\
&\beta_3=\frac{1}{2\rho U_j^2} \\
&\beta_4=\frac{1}{8}\lambda+2\alpha_{12}-\frac{1}{16} \\
&\beta_5=\frac{1}{8}\lambda^2+3\alpha_{12}\lambda+2\alpha_{22}-\frac{1}{16}\lambda-\frac{1}{2}\alpha_{12} \\
&\beta_6=\frac{1}{8\rho U_j^2}=\frac{1}{4}\beta_3 \\
&\beta_7=\frac{1}{2} \\
&\beta_8=\frac{1}{2}\lambda+\alpha_1 \\
&\gamma_1=-\frac{1}{2}\frac{\rho'}{\rho}\lambda^2-2\alpha_1\frac{\rho'}{\rho}\lambda-\alpha_2\frac{\rho'}{\rho} \\
&\gamma_2=-\frac{9}{32}\frac{c^2}{a}-\alpha_{12}\frac{\rho'}{\rho}\lambda-\alpha_{22}\frac{\rho'}{\rho}+\frac{1}{16}\frac{\rho'}{\rho}\lambda+\frac{1}{2}\frac{\rho'}{\rho}\alpha_{12} \\
&\gamma_3=-\frac{\rho'}{\rho}\left(\frac{1}{2}\lambda+\alpha_1\right)
\end{aligned}\right\} \tag{21}$$

Hence, by determining the coefficients of equation (21), equation (20) can be solved numerically as a simultaneous differential equation. For the determination of the initial values of the coefficients in equation (21), we will describe a method in the following for λ.

6.2 Initial Values of λ

For the ratio of the flow rate m_1 in the mixing tube at a distance x in the axial direction to the momentum M, at the same distance , we can write the following, for the range $\lambda > 0$.

$$\frac{m_1}{M_1}=\frac{2\pi a^2\int_0^1\rho u\eta d\eta}{2\pi a^2\int_0^1\rho u^2\eta d\eta}=\frac{\left(\frac{1}{2}\lambda+\alpha_1\right)(\lambda+1)}{U_m\left(\frac{1}{2}\lambda^2+2\alpha_1\lambda+\alpha_2\right)} \tag{22}$$

/21

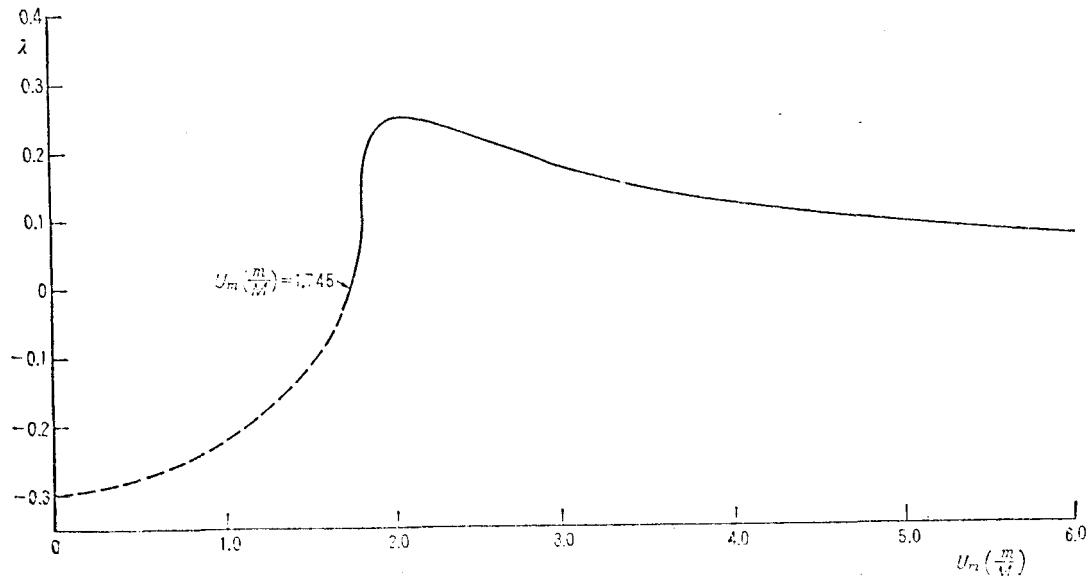

Figure 22. Values of Early Stage of λ.

Hence, plotting $U_m(m_1/M_1)$ or $U_m(m/M)$ (where 2m is the flow rate per unit area, and 2M is the momentum per unit area) along the abscissa, and the values of λ which satisfy the physical condition $0 < \lambda << 1$ among those which satisfy equation (22) along the ordinate, we obtain the curve shown by the solid line in Figure 22.

When the range is extended to $\lambda < 0$, we must give consideration to the part which gives counterflow, and replace equation (22) by

$$\frac{m_1}{M_1} = \frac{2\pi a^2 \int_0^1 \rho u \eta \, d\eta}{2\pi a^2 \left(\int_0^{\lambda_0} \rho u^2 \eta \, d\eta - \int_{\lambda_0}^{1} \rho u^2 \eta \, d\eta \right)} \tag{23}$$

where, among the roots λ_o of equation (24) (at u = 0) we have those which satisfy the physical condition $0.5 \leq \lambda_o \leq 1.0$.

$$2\lambda_0^3 - 3\lambda_0^2 + (1 + \lambda) = 0 \tag{24}$$

Therefore, the dotted line in Figure 22 represents the values of λ which satisfy equation (23).

From Figure 22, the values of λ just prior to mixing can be obtained from experimentally obtained $U_m(m/M)$. In the following, a method for the determination of $U_m(m/M)$ is described.

6.3 Determination of $U_m(m/M)$

In an experiment, m can be found directly from the primary and the secondary air fluxes. From the measured wall pressure distribution, the change in momentum

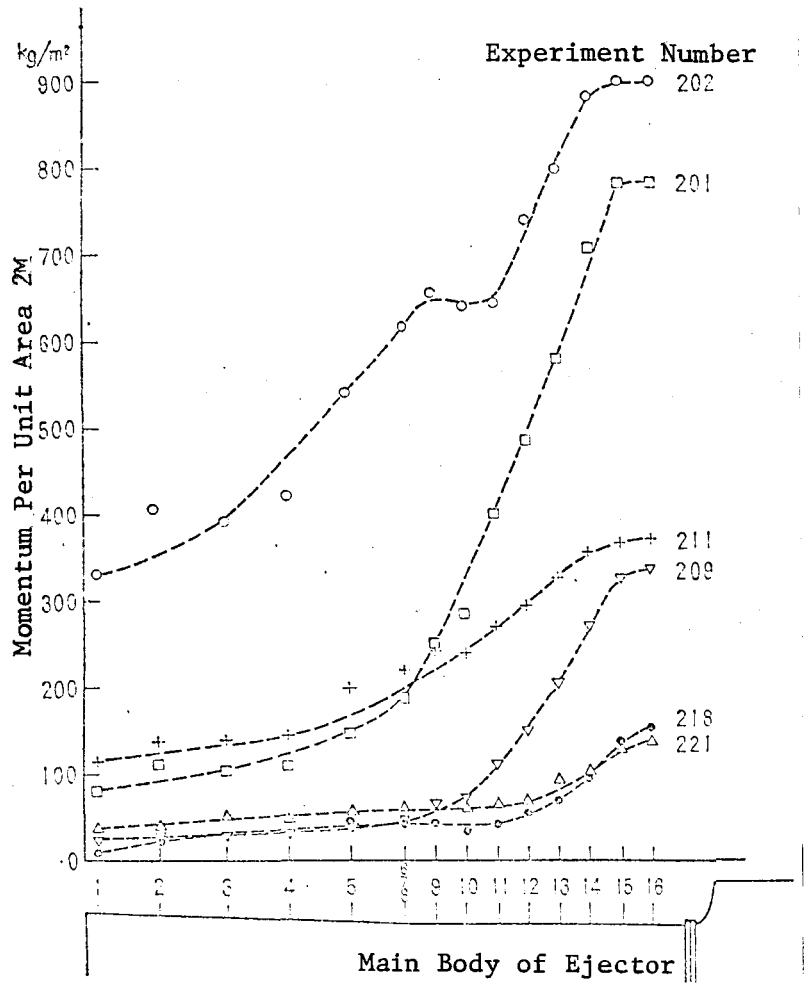

Figure 23. Change in Momentum.

can be calculated, assuming that mixing is completed at the ejector outlet, and that it is being discharged to the atmosphere as a uniform flow. Typical examples are shown in Figure 23. From such figures, M and hence (m/M) can be found. In the following, the initial values of U_m are examined. For convenience, the authors have rearranged the numerical values from the theoretical analyses conducted by Squire and Torouncer (Ref. 6) on an imcompressible fluid ejecting into a free stream, and have presented the results in Figure 24. In the figure, U_o is the free stream velocity, U_1 is the ejecting velocity, and $\bar{C}$ is obtained by dividing the distance from the ejector outlet to the tip of the potential core by the nozzle radius. Although the conditions of the fluid which is treated here are different from those used in the calculations for Figure 24, the potential length in this experiment appears to be approximately 6~9 times the nozzle radius. Since this length approximately corresponds to where the static pressure rise starts in the mixing tube, the initial values of U_m can be expressed by the potential jet velocity leaving the nozzle. The initial values, therefore, can be determined from the static pressure of the chamber, and also from the total pressure and temperature just prior to nozzle ejection.

/22

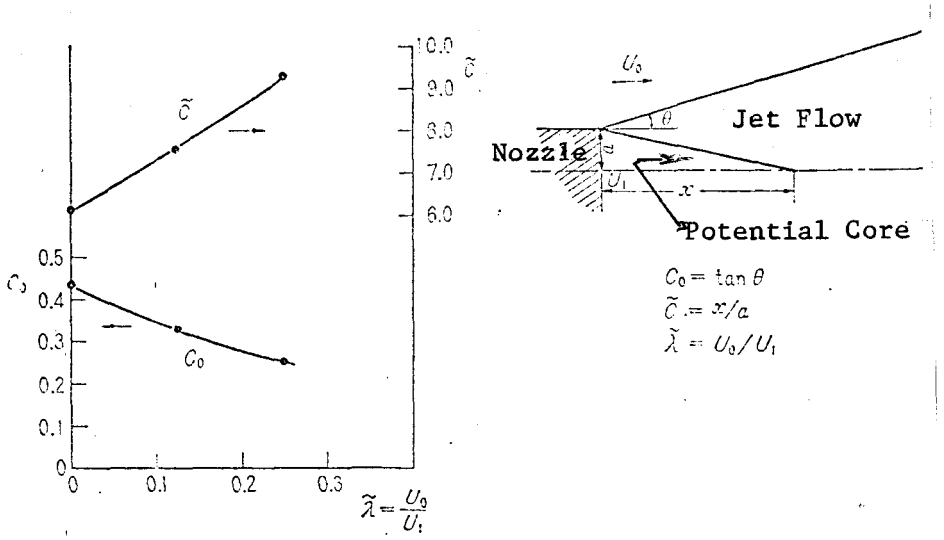

Figure 24. Discharge Angle and Length of Potential Core.

6.4 Calculated Values of Mixing Length

In order to find mixing length 1, the proportionality constant c must be determined. The constant depends only on $\gamma 2$ among the coefficients in equation (21). As stated before, when U_m(m/M) is determined in an experiment, then the initial value of λ and hence the value of U_j are known. Further, by assuming a value for c, the changes in velocity and pressure along the mixing tube can be calculated from equation (20). In the static pressure distributions in Figures 14 - 19, only the mixing tube parts are plotted in Figure 25(a) - (f). The solid lines are the calculated static pressures. The parameters shown, such as 0.12, 0.15, 0.11 are the value of the proportionality constant c for the mixing length, which varies in the range from 0.10 to 0.25. When the primary air flux is rather small as in Experiment Numbers 139, 137, 131, 129 in Figure 25(a), the proportionality constant is approximately constant throughout the mixing tube. Nevertheless, when supersonic conditions exist only locally after being ejected from the nozzle, as in Experiment Number 116, c must be expressed as a function in the flow direction in order to find agreement with experiment. For the convenience of calculation, a method was adopted in which calculations were carried out initially by letting c be a constant, which was then varied in a stepwise fashion, as the deviation from experiment became significant. Except for a few cases, the experimentally obtained c appears to lie between 0.11 to 0.18. Wang (Ref. 8) reports a value of c = 0.14 at the center of the tube. At any rate, as is often indicated, the mixing length is very characteristic to the experiment. In these internal flows, although c may vary in the radial direction, the analyses were carried out by disregarding any variation in the direction normal to the tube axis because of the assumptions made at the beginning that static pressure and density are invariable in the radial direction. The mixing length, therefore, must be interpreted as the average value of the mixing length in the radial direction.

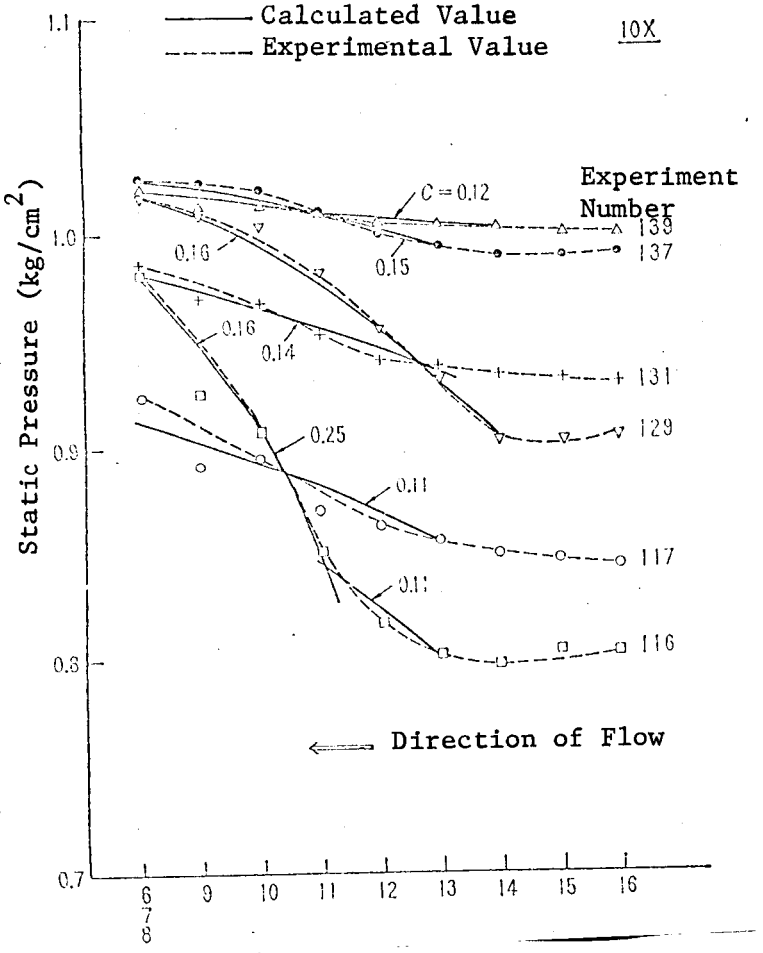

Figure 25(a) Mixing Distance Ratio Constant and Rise in Static Pressure (d-200, 1=200).

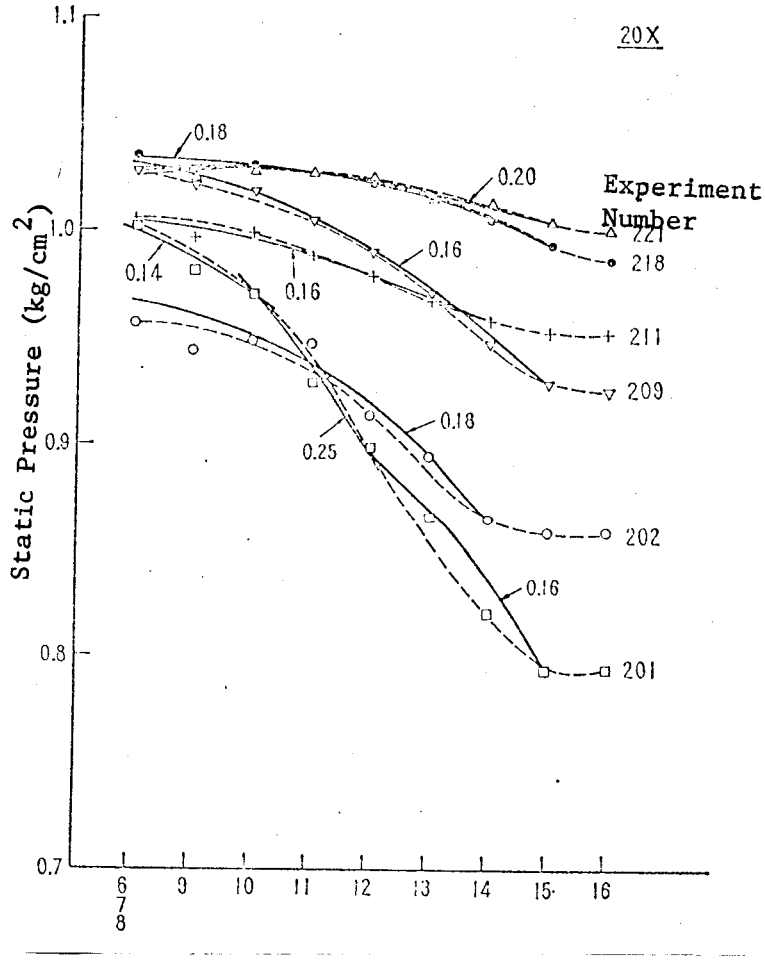

Figure 25(b) Mixing Distance Ratio Constant and Rise in Static Pressure (d=200, 1=600).

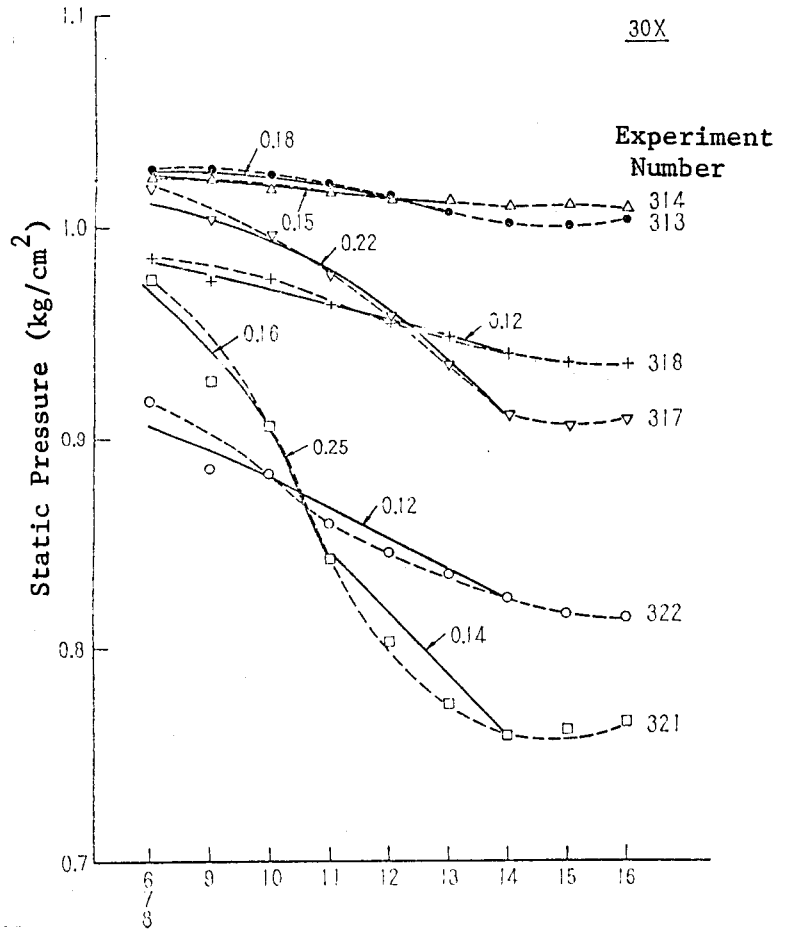

Figure 25(c) Mixing Distance Ratio Constant and Rise in Static Pressure (d=230, l=200).

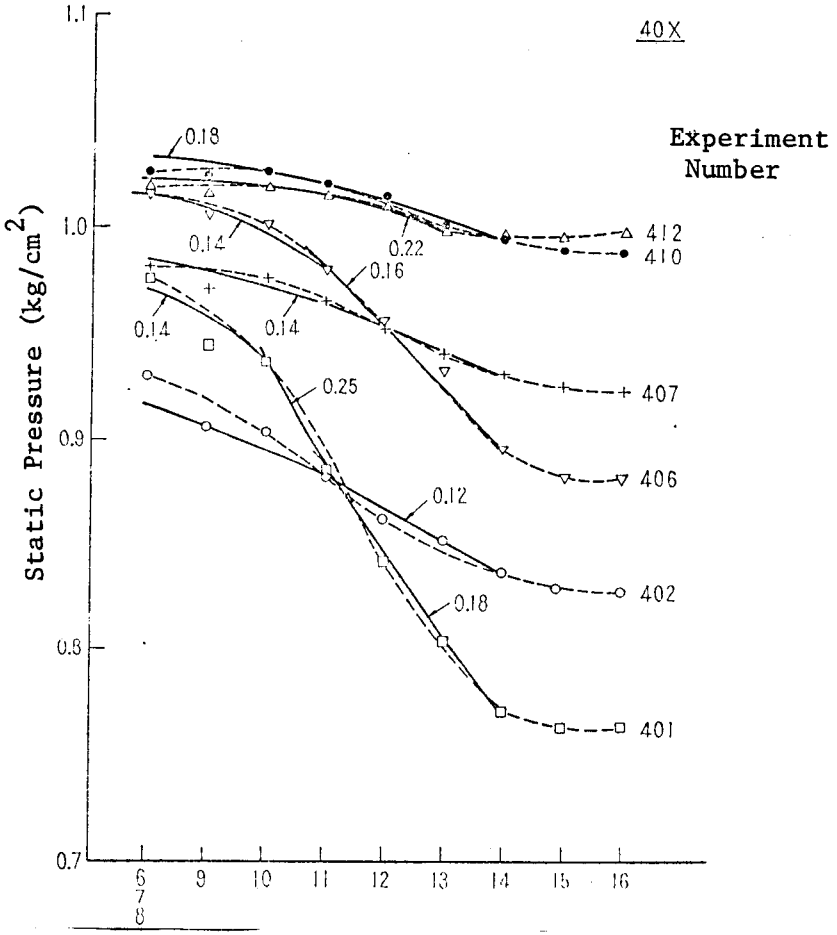

Figure 25(d) Mixing Distance Ratio Constant and Rise in Static Pressure (d=230, l=430).

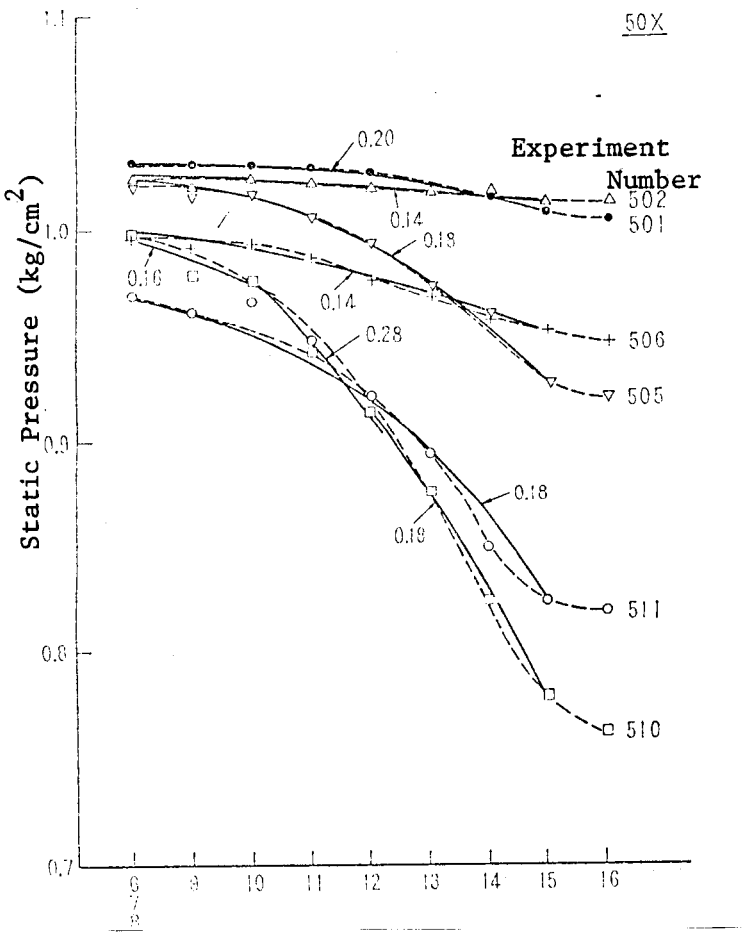

Figure 25(e) Mixing Distance Ratio Constant and Rise in Static Pressure (d=230, l=660).

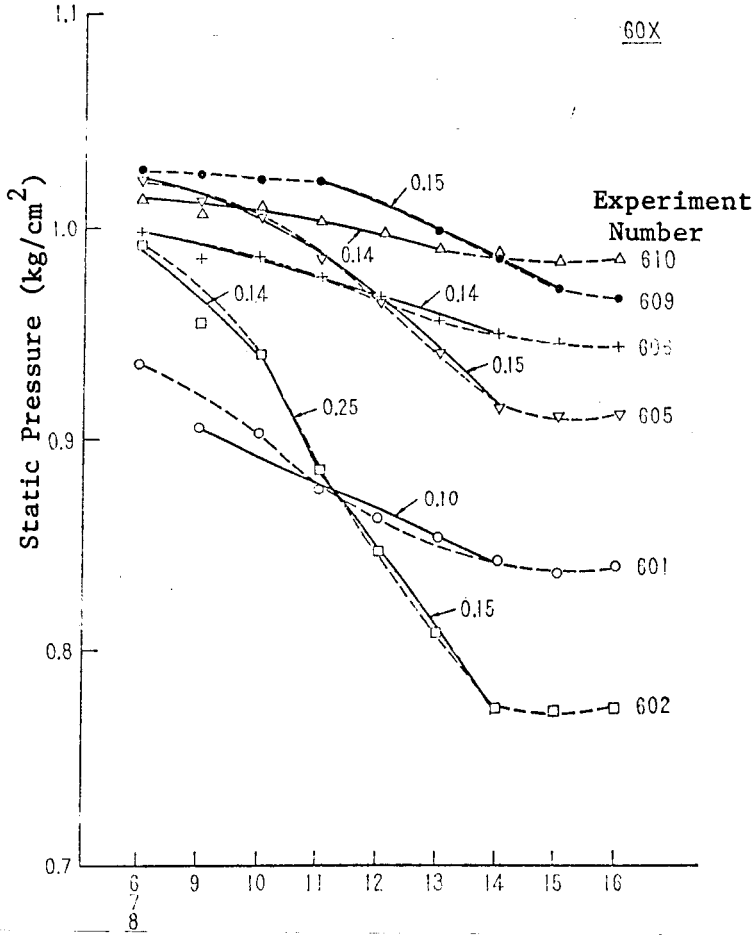

Figure 25(f) Mixing Distance Ratio Constant and Rise in Static Pressure (d=200, l=400).

6.5 Total Pressure Distribution

/27

Part of the results for the total pressure in the radial direction measured by installing comb-shaped Pitot tubes at the inlet and outlet of the mixing tube are shown in Figure 26 (a)-(c). Static pressures are marked at the tube wall. Even the rather steep pressure distribution at the inlet flattens out at the outlet. This is seen also in the static pressure rise along the mixing tube, which becomes saturated near the outlet, indicating almost complete mixing. If the secondary air flux is almost a maximum when the primary flux is a maximum -- that is, when the air flux is near maximum for the ejector (corresponds to Experiment Numbers 202, 322, 402, 509, 601 in the figures) -- the pressure distribution of the flow into the diffuser continues to show a rise in the radial direction without being completely mixed in the parallel pipe. This result is understandable considering the rather steep static pressure rise seen at the straight pipe outlet, compared to the pressure distributions in Figures 15 - 19.

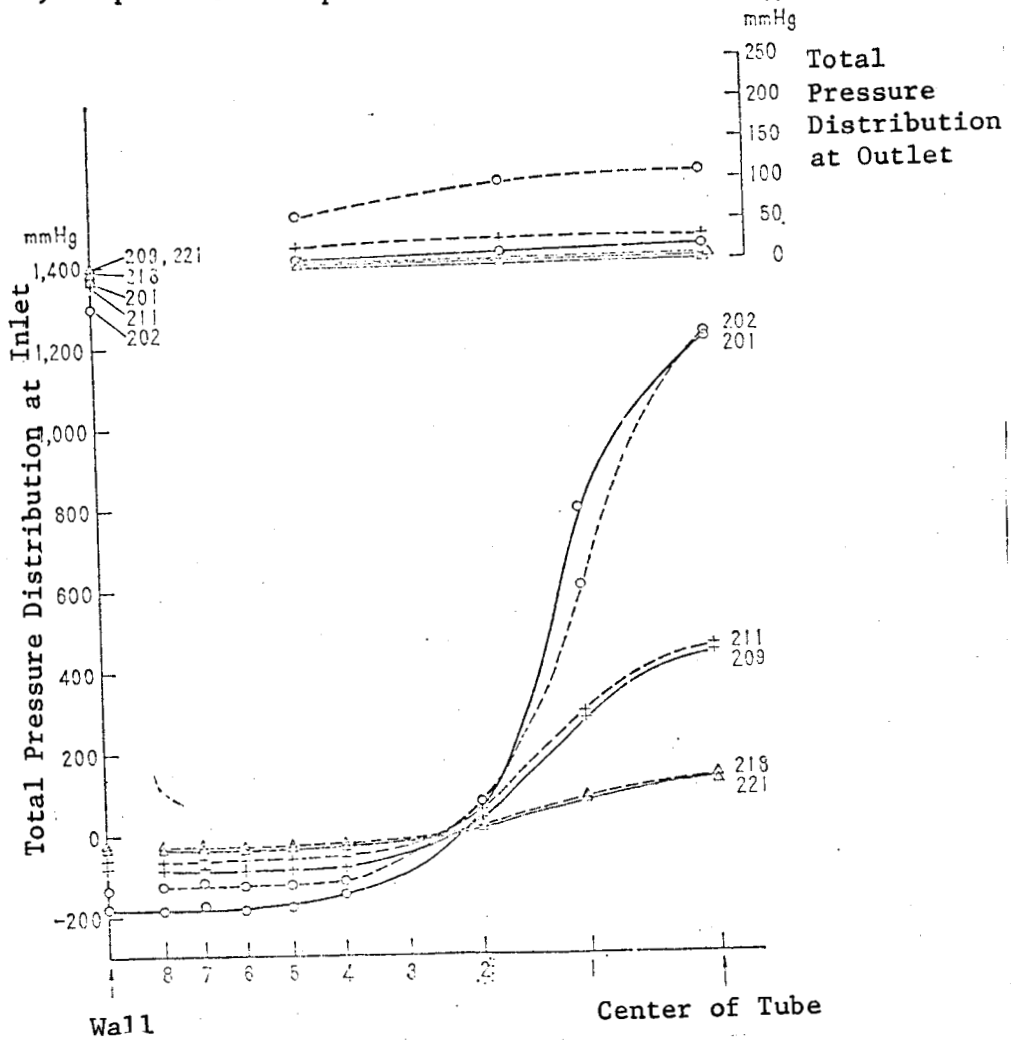

Figure 26(a) Distribution of Total Pressure in Mixing Tube. (d=200, l=600).

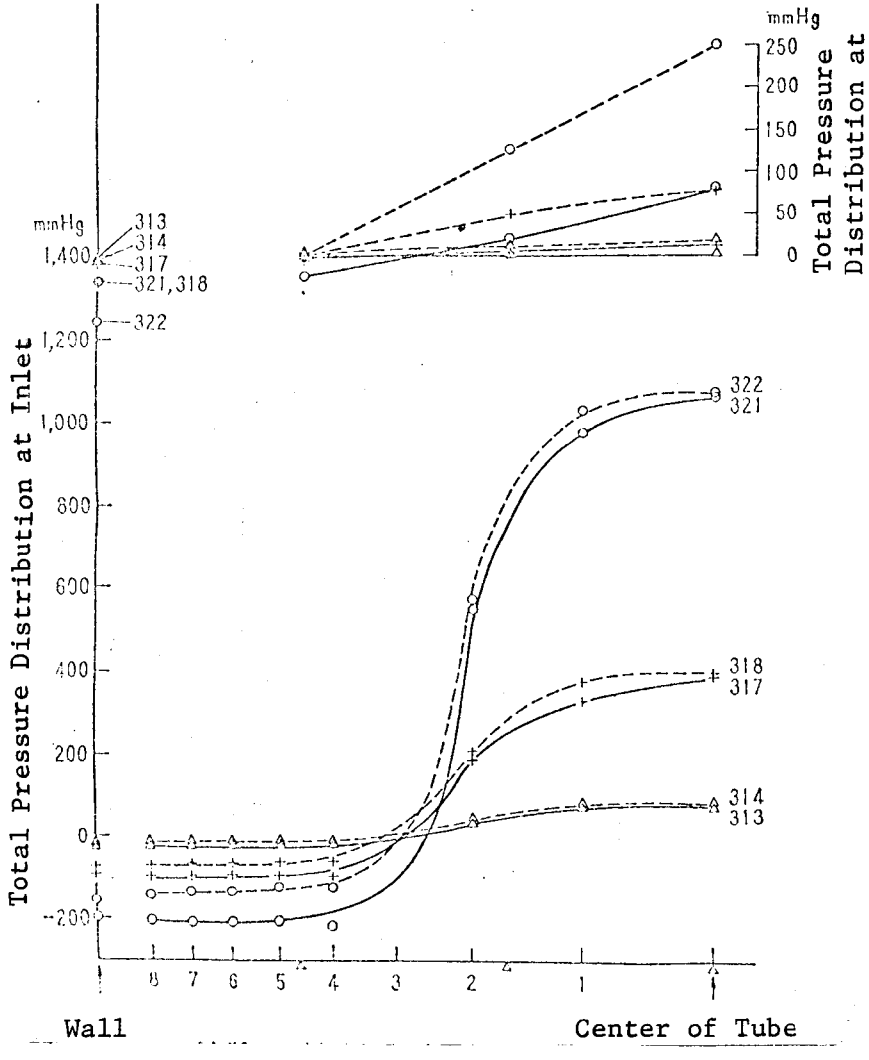

Figure 26(b) Distribution of Total Pressure in Mixing Tube (d=230, l=200).

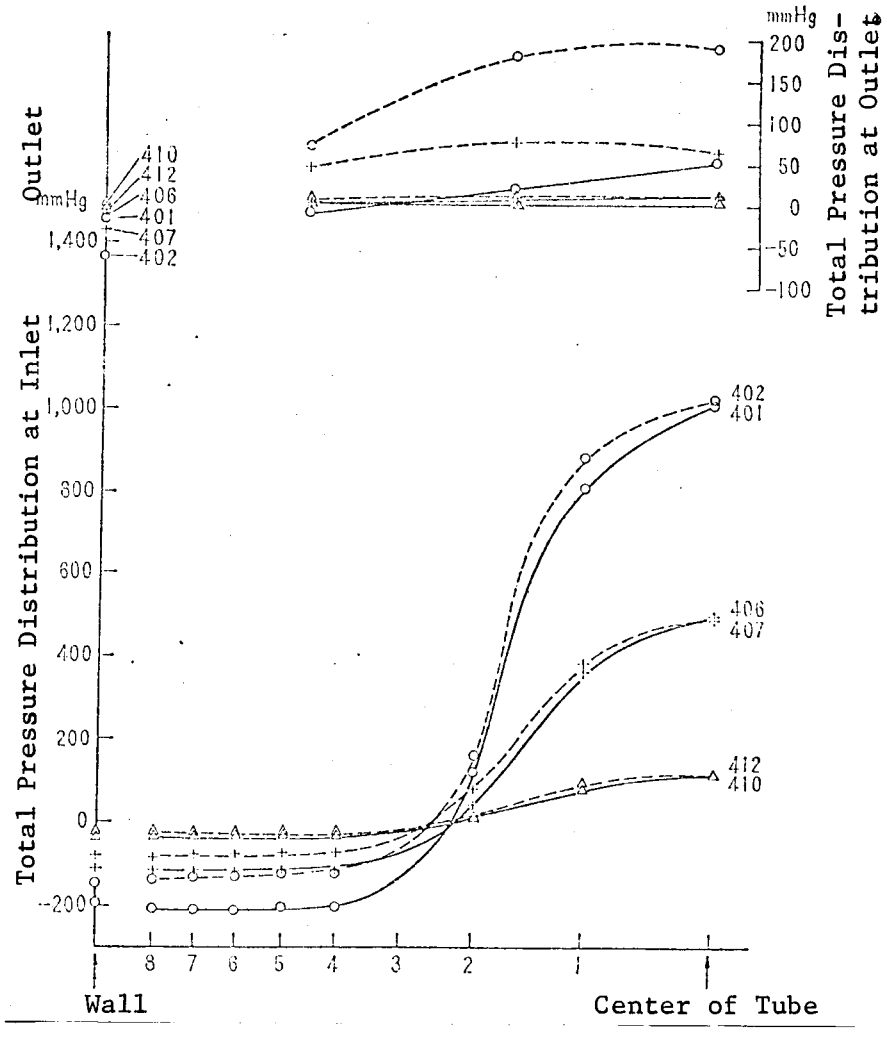

Figure 26(c) Distribution of Total Pressure in Mixing Tube (d=230, l=430).

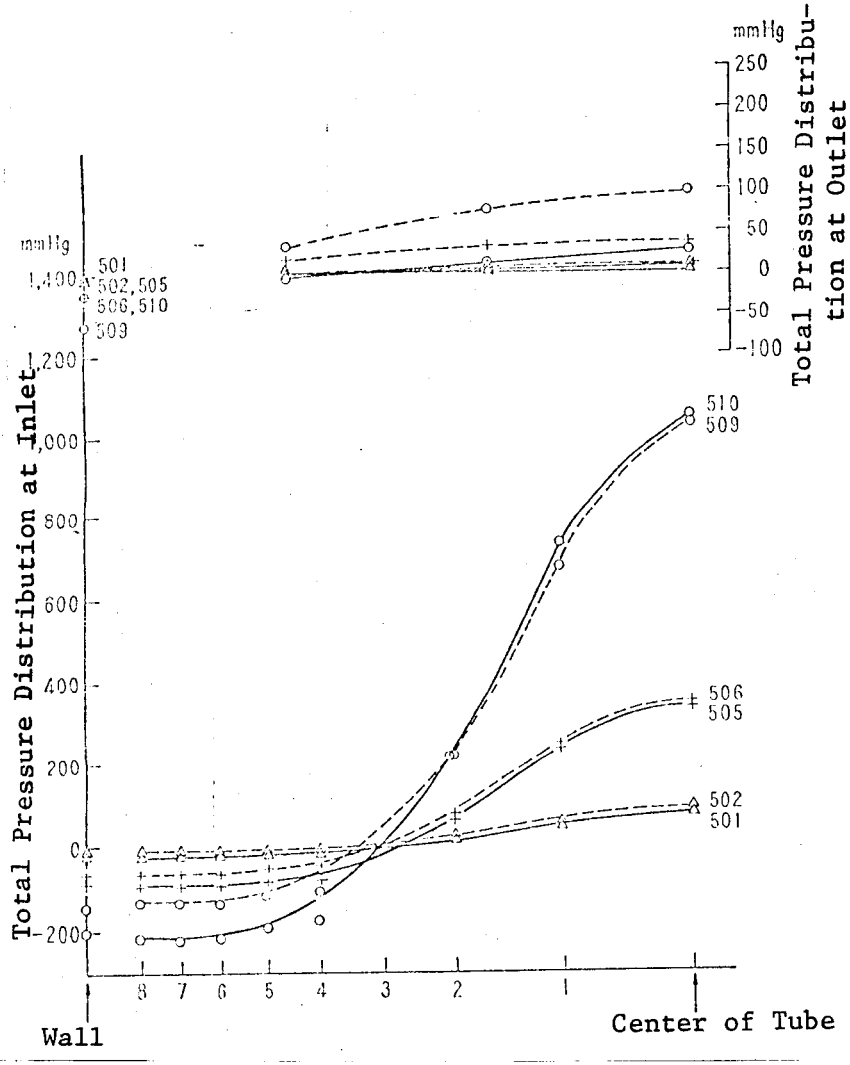

Figure 26(d) Distribution of Total Pressure in Mixing Tube (d=230, l=660).

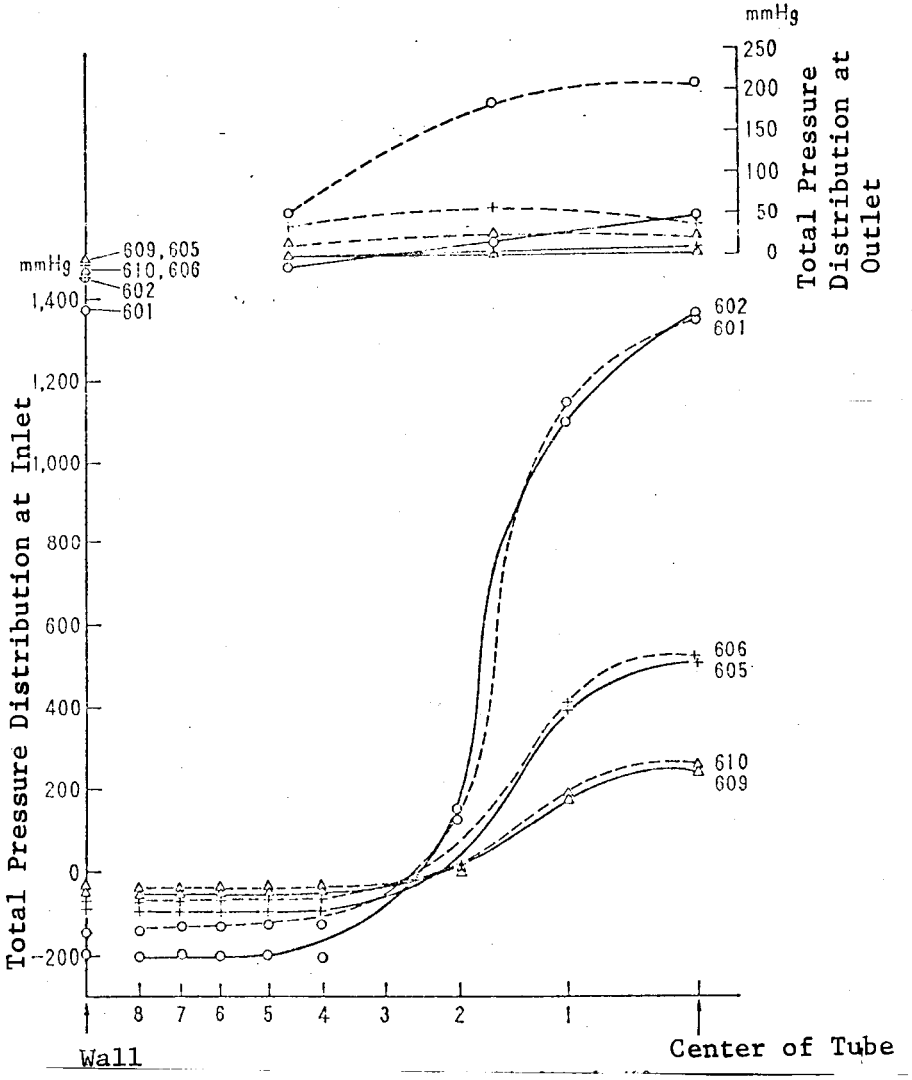

Figure 26(d) Distribution of Total Pressure in Mixing Tube (d=200, l=400).

7. Conclusion /30

In order to obtain a high speed axial velocity for the testing of the single-stage axial flow compressor, a large scale air ejector was developed. The performance curve was obtained by carrying out experiments for six different combinations by changing the nozzle diameter, and the length from the nozzle tip to the mixing tube. The design based on the data from the existing small air ejector was used. When the primary air flux (the driving air flux) was 21.2 kg/sec, the flux ratio was 0.95, that is, the secondary flux (the intake air flux) was a maximum flux of 20.1 kg/sec. The maximum vacuum, on the contrary, was -207 mm Hg (gauge pressure). We also found that the difference between the large and the small Reynolds number is not significant.

Attention was also focused on the mixing phenomenon which is the primary function of ejectors. Experimental data, such as the static pressure distributions, and the total pressure distributions, for the mixing process in parallel tubes were obtained, from which the average calculated mixing lengths in the radial direction were found to be approximately 0.1～0.2 times the radii of the mixing tubes.

We are indebted to Masakatsu Matusmoto the Department Manager, Tadao Shimazaki the Section Manager, and Yasuji Katayama who have given their assistance in the experiments.

REFERENCES

1. Surendraiah, M., and RaO, D. Performance of a Two-Dimensional Center-Jet Ejector, NAL Bangalore, TN-AE-18-63, 1963/7.
2. Kastner, L., and Spooner, J. An Investigation of the Performance and Design of the Air Ejector Employing Low-Pressure Air as the Driving Fluid, Proc. Inst. Mech. Engrs., 140, 149, 1950.
3. Manganiello, J., and Bogatsky, D. An Experimental Investigation of Rectangular Exhaust-Gas Ejectors Applicable for Engine Cooling, NACA Report Number 818.
4. Pai, S. Axially Symmetrical Jet Mixing of a Compressible Fluid, Quarterly Appl. Math., Vol. X, No. 2, PP 141-148, 1952/7.
5. Burley, R.R., and Bryant, L. Experimental Investigation of Coaxial Jet Mixing of Two Subsonic Streams at Various Temperature, Mach Number and Diameter Ratio for Three Configurations, NASA Memo 12-21-58E.
6. Squire, H., and Torouncer, J. Round Jets in a General Stream, R. & M., No. 1974, 1944/1.
7. Hill, P. Turbulent Jets in Ducted Streams, J. Fluid Mech., Vol. 22, Part 1, PP 161-186, 1965/5.
8. Wang, C. On the Velocity Distribution of Turbulent Flow in Pipes and Channels of Constant Cross Section, J. App. Mech., A85-A90, 1946.
9. Tsutomu, Miyata. The Low Pressure Air Ejector, Ehara Report, Vol. 11, No. 42, PP 59-64, 1962.
10. Yoiichi, Takashima, and Hasegawa, Masayuki. Studies on the Air Ejector, Kagakukogaku (Chemical Engineering), Vol. 15, No. 9, PP 427-438, 1954.
11. Watanabe, Ichiro, Watanabe, Tsuyoo, Nahata, Tetsu, and Nakagawa, Hiroshi. Experimental Studies on the Air Ejector. Report No. 2, Jo. of Japan Mechanical Engineering Soc., Vol. 22, 120, PP 590-595, 1956.

12. Watanabe, Ichiro, Watanabe, Tsuyoo, and Ando, Tei. Experimental Studies on the Air Ejector, Jo. of Japan Mechanical Engineering Soc., Vol. 22, No. 120, PP 596-602, 1956.
13. Barchilon, M., and Curtet, R. Some Details of the Structure of an Axisymmetric Confined Jet With Backflow,ASME, Series D, Vol. 86, No. 4, PP 777-787, 1964/10.
14. Addy, A., and Chow. W. On the Starting Characteristics of Supersonic Ejector Systems, ASME, Series D, Vol. 86, No. 4, PP 861-868, 1964/10. /31
15. Curtet, R., and Ricou, F. On the Tendency to Self-Preservation in Axisymmetric Ducted Jets, ASME, Series D, Vol. 86, No. 4, PP 765-776, 1964/10.

Appendix I Ejection in a Free Stream

Since a theory was developed in (Ref. 6) for a ducted flow whose velocity profile is approximated by a third order equation, we will consider ejections in a free flow which is accompanied by a uniform flow.

Assuming that the static pressure rise is $dp/dx \simeq 0$, and neglecting the frictional forces at the boundary of the free flow and the jet, the following relation is obtained (c.f. Appendix Figure 1),

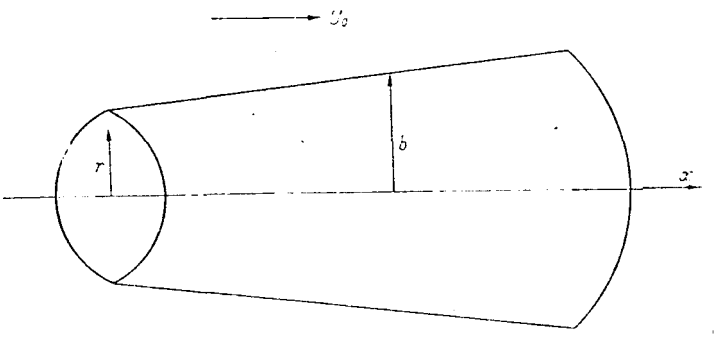

Supplementary Figure 1. Flow Emitted Toward Center of Free Flow.

$$2\pi\frac{d}{dx}\left[\int_0^b \rho u^2 r\,dr\right]dx=\rho\cdot 2\pi b U_0^2 db \tag{A-1}$$

where U_o is the free flow velocity, and b is the jet radius at the cross section under examination, which is generally a function of x. By approximating the axial velocity u by a third order equation in r as in (Ref. 6), and letting $\partial u/\partial r = 0$ at $r = b$, and $\partial u/\partial r = 0$ at $r = 0$, we obtain

$$u-U_0=2\lambda_1 r^3-3\lambda_1 b r^2+\lambda_1 b^3 \tag{A-2}$$

$$\lambda_1=\frac{U_m-U_0}{b^3} \tag{A-3}$$

where referring to Appendix, Figure 1, although U_m generally is a function of x, U_o is regarded as a given constant. Substitution of (A-2) into (A-1), and restricting ourselves to the incompressible case in order to obtain simple analytical

solutions, results in

$$\frac{1}{35}\frac{d}{dx}[(U_m-U_0)^2b^2]+\frac{1}{10}U_0\frac{d}{dx}[(U_m-U_0)b^2]=0 \qquad \text{(A-4)}$$

Assuming b can be expressed as follows, using an experimentally determined constant c_1, we find

$$b=c_1x \qquad \text{(A-5)}$$

Then equation (A-4) can be integrated as follows: /32

$$x^2U^2+\frac{7}{2}U_0x^2U+c_2=0 \qquad \text{(A-6)}$$

where c_2: integration constant; U: $U_m - U_o$

Assuming that the velocity profile can be approximately expressed by a third order equation at $x-l_1$ after leaving the nozzle, where x is measured from an imaginary origin, and also that the tip of the potential with velocity V_j is maintained at that point, we can write $U_{x=l_1} = V_j - U_o$

Hence, the integration constant is obtained as,

$$c_2=-\left(l_1^2S^2+\frac{7}{2}U_0l_1^2S\right) \qquad \text{(A-8)}$$

where

$$S=U_{x=l_1}=V_j-U_0 \qquad \text{(A-9)}$$

Hence, from equation (A-6), we have

$$U=-\frac{7}{4}U_0+\sqrt{\frac{49}{16}U_0^2+\left(S^2+\frac{7}{2}U_0S\right)\eta} \qquad \text{(A-10)}$$

where

$$\eta=\left(\frac{l_1}{x}\right)^2 \qquad \text{(A-11)}$$

By substituting equation (A-10) into (A-2), the velocity distribution can be expressed as,

$$u=\left[-\frac{7}{4}U_0+\sqrt{\frac{49}{16}U_0^2+\left(S^2+\frac{7}{2}U_0S\right)\eta}\right] \qquad \text{(A-12)}$$

$$\left[\left(\frac{2}{c_1^3}\right)f^3-\left(\frac{3}{c_1^2}\right)f^2+\right]+U_0$$

where

$$f=\frac{r}{x} \qquad \text{(A-13)}$$

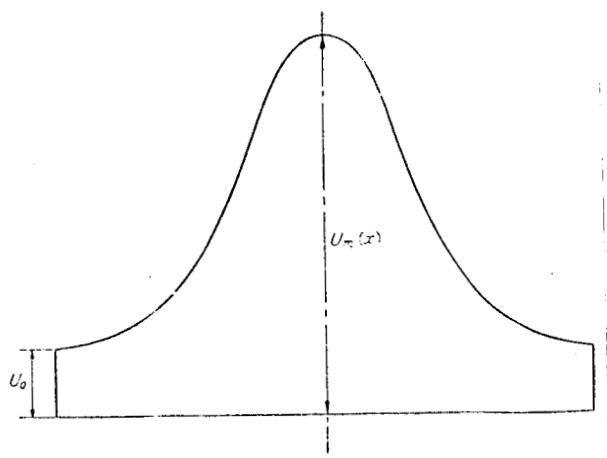

Supplementary Figure 2. Velocity Distribution.